Science & Technology Facilities Council

Technical Report
RAL-TR-2009-009

Monte-Carlo simulation of the primary spectrometer on the proposed FIRES instrument

C Pelley

2009

RAL Library
Science and Technology Facilities Council
Rutherford Appleton Laboratory
Harwell Science and Innovation Campus
Didcot
OX11 0QX

Tel: +44(0)1235 445384
Fax: +44(0)1235 446403
email: library@rl.ac.uk

ISSN 1358-6254

Monte-Carlo simulation of the primary spectrometer on the proposed FIRES instrument

Carwyn Pelley

Contents

1 Abstract

Optimization of guide design for the proposed neutron backscattering instrument FIRES is discussed in this report, concluding that elliptic non-symmetric geometry being the most suitable for maximizing transmission. Comparison with the OSIRIS and IRIS instrument at ISIS is made. Significant gain is shown in the optimization of a simple linearly tapered curved guide with a gain of $\times 2.3$ over a $(2 \times 3)cm^2$ sample area compared to the IRIS instrument. However, further gain is shown with elliptic tapering with $\times 3.9$ over the $(2 \times 3)cm^2$ sample area. Yet further gain is also achieved with taking elliptic geometry to the full length of the guide from the biological shielding in the vertical while keeping curvature in the horizontal, with a gain of $\times 4.1$. Further investigation however is required in the non-symmetric elliptic from moderator option, with modification of the biological shielding due to an indicated gain in excess of $\times 12$ (increase of $> \times 3$ compared to the best set-up without biological shielding modification).

2 Introduction

2.1 Scientific case

The proposed FIRES instrument offers to extend the number of applications that can be investigated at the ISIS facility with its high flux and μeV resolution capabilities, together with a large dynamic range (range of accessible energy transfers). Some of the many applications that the FIRES instrument is to open to the neutron scattering community as described by Demmel and Andersen [1] include Hydrogen storage, glasses and complex liquids, quantum magnetism, and confined fluids. Such areas of research have been discussed in brief already (see dissertation, Section 2.5, Appendix B). The instrument is to use a coupled moderator normally associated with lower resolution (wider curve) and high intensity. Altering the moderator pulse width can be achieved with the use of a pulse shaping chopper (PSC) as described by Demmel and Andersen [2] allowing the resolution to be increased by narrowing the pulse width, while retaining the higher intensity characteristics of such a moderator. The optimization and design of the FIRES instrument is key for the next generation of instruments similarly being built at other sources as discussed in Section 3.1.1 and 3.1.2.

2.2 Monte-Carlo

Neutron scattering is a low signal techniques due to its relatively low flux levels. Hence it is especially important to optimize instrument design and parameters through neutron ray-trace simulations such as McStas. Analytical methods are often used as a basis for a low number of optical elements by the use of phase-space theory. This reaches its limit with a high number of optical elements, due to increased coupling between neutron parameters becoming ever stronger as discussed by Willendrup P. [3].

The Monte-Carlo technique is used in the determination of numerical solutions to problems that cannot be solved analytically, as such, it is required in the design and optimization of complex geometrically shaped instruments. McStas works by the principle of probability (Monte-Carlo sampling) where neutron scattering events for example are integrated over all neutron trajectories resulting in estimates of measurable quantities. An example of the Monte-Carlo method for the determination of an integral is shown below as described by Willendrup P. [3]. The integral is solved at 'n' random points (avoiding bias) and summing these values, gives a numerical approximation to the integral;

$$\lim_{n \to \infty} \frac{1}{n} \sum_{i=1, a \leq u_i \leq b}^{n} f(u_i) = \frac{1}{b-a} \int_a^b f(u) du \tag{1}$$

Where 'u_i' is a randomly chosen value according to Monte-Carlo sampling in which '$f(u)$' is a finite continuous integral function with limits between 'a' and 'b'.

2.2.1 McStas neutron ray tracing package

McStas is a fast and versatile neutron ray-tracing simulation software that offers the ability to determine accurate estimates for flux, resolution, optimization of parameters and

designs where analytical estimates cannot be used. Based on a meta-language specifically designed for neutron scattering, it is translated efficiently into ANSI-C which is then translated into an executable, which performs the simulation. The meta-language allows the building of an instrument from individual components, where a library of standard components is included as part of McStas. Such components can be designed by the user by their own specifications and then used in their instrument. An obvious advantage of neutron ray-tracing simulation is the ability to place monitors at any desired location(s) without influencing the beam if chosen.

2.2.2 The Neutron Weight and statistical uncertainty

McStas uses the idea of neutron weighting in order to perform fast simulations of complex instruments with large statistics. Neutron rays are assigned with a weight, and these weightings are adjusted according to their path. This means for example, a number of rays entering a component of a certain reflectivity, results in all rays reflecting in the component only that their weighting is adjusted according to this reflectivity. By this method, all rays are kept and lower statistics may be used in Monte-Carlo simulations. In a real experiment of such an instrument, only those neutrons that reflect would then be used, meaning that the neutrons up until that point are wasted. By this method a re-adjustment of the weighting is usually made between 0-1, resulting in a loss in flux throughout the instrument. The Monte-Carlo approach to simulation is that the neutron weight is adjusted to resemble the behaviour of real physical properties.

The weight representation can be made as follows;

$$p_n = p_0 \sum_{j=1}^{n} \pi_j \tag{2}$$

Where 'p_0' denotes the initial weight, 'p_n' the final weight after traversing through the instrument and 'π' the multiplication factor for the 'j^{th}' component.

"The sum of these weights is an estimate of the mean number of neutrons hitting the monitor (or detector) per second in a real experiment" as discussed by Willendrup P. [3]. This mean number of neutrons hitting the detector is the intensity.

$$I = \sum_i p_i = N p_{av} \tag{3}$$

Where 'p_i' is the weight of the i'th neutron ray, 'N' the number of neutron rays and 'p_{av}' the averaged neutron weight.

This leads to an approximate statistical uncertainty of;

$$\sigma(I)^2 \approx \sum_i p_i^2 \tag{4}$$

It is described also that the central limit theorem provides an estimate for the error on evaluating integrals for large enough statistics by $1/N$.

3 Literature Review

A number of topics are discussed in the literature review for the dissertation document (Appendix B). Moderator choice as already discussed (see Appendix B Section 3.1) concluded that a coupled hydrogen moderator is the most appropriate choice to achieve high intensity, and is in agreement with Demmel and Andersen [2]. A coupled moderator is the chosen moderator also for the similar instrument DIANA at J-PARC as described in Section 3.1.1. Also discussed is the pulse shaping chopper option for shaping the coupled moderator pulse in order to achieve μeV resolution and that again the DIANA uses this method to achieve high resolution. Such an approach is novel and is considered for achieving a high resolution with a large flux for the FIRES instrument.

A typical expected design for the FIRES instrument is shown in Fig.1.

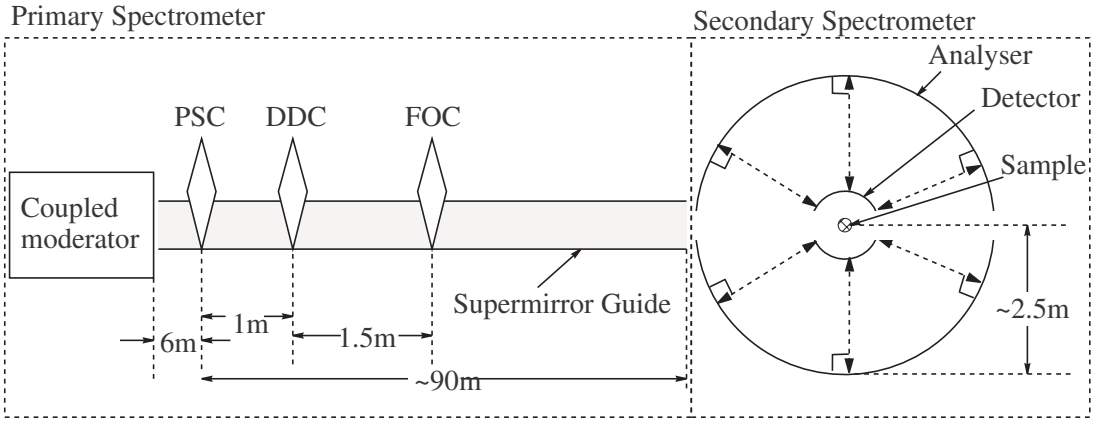

Figure 1: Illustration of the expected FIRES set-up, showing the pulse shaping chopper (PSC), double disk chopper (DDC) and frame overlap chopper (FOC).

3.1 Other instruments with similar attributes

3.1.1 DIANA at J-PARC

An instrument named DIANA is to be built at J-PARC, the 1 MW spallation neutron source in Japan (see dissertation document, Section 2.4 in Appendix B), a backscattering neutron spectrometer like the proposed FIRES to achieve μeV resolution. Its design is very similar to that expected for FIRES only with DIANA being 40m rather than 90m long (with a more powerful spallation source). It is to use a PSC to shape the pulse in order to utilize the higher intensity of a coupled moderator, together with the short pulse length necessary to achieve μeV resolution as described by Takahishi N. et al. [4]. This achieved by removing the tail. This 40m long guide, has geometry which is elliptical in the vertical plane for achieving maximum transmission at the sample position and then curved geometry in the horizontal so that direct line of sight is lost between the moderator and sample. This prevents fast neutrons from the moderator that are not absorbed by the

choppers from reaching the sample position and thus do not contribute to the background signal. A detailed presentation made on the design and expected performance is discussed by Takahishi N. et al [5].

3.1.2 BASIS at SNS

An already built instrument capable of μeV resolution neutron scattering as already discussed (see dissertation document, Section 2.4 in Appendix B). This instrument at the spallation source SNS is called BASIS [6]. The design however is different to that of the proposed DIANA or FIRES as the SNS accelerator provides the most intense pulsed neutron beams in the world with a power of 1.4 MW. High resolution is achieved from a poisoned moderator, and the higher power rating accelerator means that high intensity can still be achieved with the use of this moderator. The design of BASIS at SNS enables a resolution of $3.5\mu eV$ full width at half maximum (FWHM). A detailed explanation of moderator types is already discussed (see dissertation document, Section 3.1 in Appendix B).

3.2 Current instruments at ISIS

Current energy resolutions available from similar instruments at the ISIS spallation source are, $24\mu eV$ and $16.5\mu eV$ FWHM for the OSIRIS and IRIS instruments respectively with the use of a PG002 analyser as discussed by Telling M. [7]. Results were simulated from Monte-Carlo simulation using VITESS software with results being in close agreement with experimental data as shown in Fig.2. These guides are simple ballistic guides (rectangular geometry guide with the possibility of linear tapered converging/diverging sections for increasing the cross-section of the guide [8]), and are described in further detail in Section 5.1.

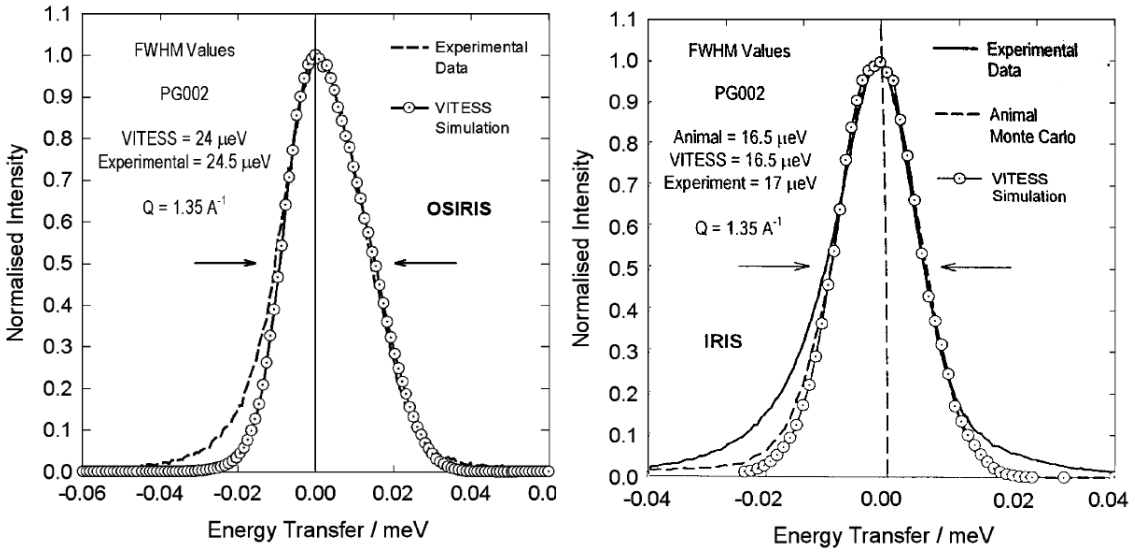

Figure 2: Instrument energy resolution function with a PG002 analyser [7].

3.3 Guide geometry overview

Elliptic guide geometry is at the cutting edge in modern guide design to maximize transmission, it being mathematically superior with the least number of reflections occurring. A comparison between parabolic, elliptic and standard ballistic was compared by Schanzer C. et al. [8] with a custom made multi tapering component as described in Section 4.4.1. As discussed in dissertation document (see Section 3.2 Appendix B), a comparison between these geometries were made by Shanzer C., showing that elliptic geometry to be the best for guide transmission together with its ability to change focal distances. Blocking fast neutrons from reaching the sample position from the source is especially important in reducing background signal. To do this, curved geometry is employed as is achieved with typical set-ups as with those mentioned above.

The next upcoming publication concerning the FIRES instrument is to be made at International Conference on Neutron Scattering Knoxville Convention Center, Knoxville, Tennessee on May 3 - 7, 2009 at Oak Ridge National Laboratory (Neutron Scattering Society of America (NSSA)) [15].

4 Theory

4.1 Optimization method

Optimization through McStas is achieved through running manual parameter scans. This method entails choosing appropriate starting parameters, then scanning each parameter in turn to find the the optimum set-up. Such a method is slow and cumbersome though has the advantage of more detailed analysis and understanding of the design. This is the method chosen for this investigation.

4.2 Definitions

Gain:
Numbers for gain throughout the results and discussion are normalized according to identical monitors on the IRIS set-up. As such, a comparison is readily made between parameter set-ups matching IRIS and OSIRIS (only 90m long).

Transmission:
Transmission is defined as the percentage of neutrons that exit the guide from those that enter it.

Divergence:
Divergence is the angle from the normal at which neutrons are incident on a particular position. An example of which is shown for the IRIS set-up in Fig.9 (page 17).

Homogeneity of divergence:
Homogeneity of divergence refers to multiple peak formation on homogeneity monitors also shown in Fig.9.

Dynamic range:
The dynamic range refers to the range of energy transfers possible (limited by the position of the PSC from the moderator).

4.3 Components

4.3.1 Moderator

Moderator design for the proposed FIRES instrument still remains in its early stages of development but for the purpose of this investigation, a coupled hydrogen moderator face from target station two (TS2) is used. The moderator resembles a 22K liquid H_2, 12x11cm face which is expected to have a time-of-flight (TOF) distribution relatively similar to that of the FIRES moderator, being rather broad but not necessarily representative of its intensity. There are a number of important variables considered in the set-up of the moderator:

E_0, E_1 - Defines the energy window of the sampled neutrons. Set to $5 - 7$Å for the purpose of guide optimization. A wider range however is considered in chopper set-up. Where the relation between energy and wavelength of the neutron is given by;

$$E = \frac{1}{2} m_n v^2$$

Where, $p = m_n v = \frac{h}{\lambda} \rightarrow v = \frac{h}{\lambda m_n}$
Hence,

$$E = \frac{h^2}{2m_n\lambda^2} \tag{5}$$

Where 'm_n' is the neutron mass and 'v' its velocity.

dist - Distance of the focus window from moderator face. This distance is to the straight guide section.

Moderator bugs - There is a "kink" in the energy distribution at around 9Å as discussed in the component manual for McStas [9] though this has no effect on this investigation with guide optimization performed around $5-7$Å and being taken out with the chopper set-up at wider energy ranges. Low statistics above 20Å are also discussed meaning that energy ranges are limited to 25Å during this investigation. A plot of the moderator pulse is shown in Fig.3.

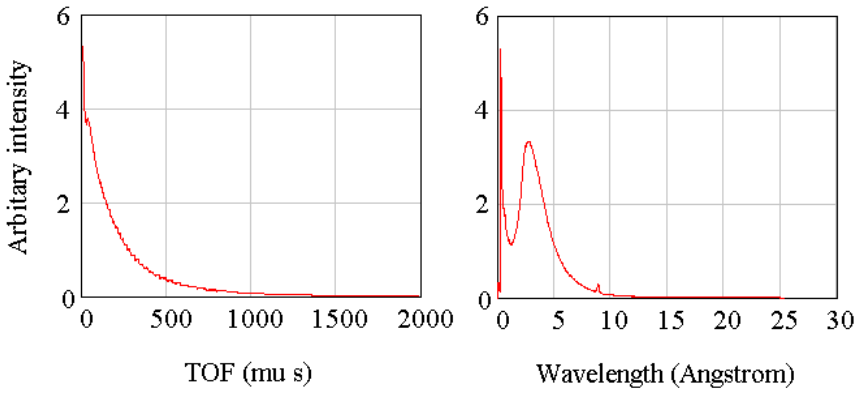

Figure 3: Simulated plot of both time of flight and wavelength distribution of the hydrogen face moderator at TS2.

4.3.2 Monitors

PSD Monitor: The PSD Monitor by Lefmann K. of Risoe, is a position-sensitive monitor that detects incident neutron rays on an x-y plane split up into pixel columns(ny) and rows(nx). This monitor is not time dependent. It also indicates the total integrated intensity across the surface of the PSD together with the error associated with it.

Divergence monitors: There are two different divergence monitors used, both created by Lefmann K., one monitor is the 1D divergence sensitive monitor which gives beam intensity as a function of horizontal divergence (deg). This then allows the detailed analysis of homogeneity at its placement position to be investigated. Rotating such a monitor also allows the vertical divergence to be monitored. The second type is a 2D divergence sensitive monitor in which intensity is measured as a function of both horizontal and vertical divergence in degrees.

TOF monitor: The TOF monitor by Nielsen K. and Hagen M. of Risoe is a rectangular monitor that measures intensity as a function of TOF.

TOF lambda monitor: This monitor by Lefmann K. is a 2D detector of intensity as a function of TOF and wavelength of neutron rays. For this, the wavelength-time distribution is readily extracted at the desired location.

Lambda and Energy monitor: These monitors by Nielsen K. and Lefmann K., are again rectangular monitors that measure the wavelength and energy of incoming neutrons respectively.

4.3.3 Standard guide component

This component, yet another created by Nielsen K., is a standard rectangular guide-piece made from four mirrors to make a guide of rectangular opening and exit, of any length. This component is the basis in which to build other components.

Optical components are defined by a number of parameters to represent real-life characteristics, of which an important aspect is reflectivity.

An important parameter which defines the optical component is the Low angle reflectivity (R_0). This is the reflectivity, where scattering occurs less than the critical scattering value. Imperfect materials render reflectivity lower than 100%. For the present investigation, this value is set to 99% (default). The critical momentum transfer (Q_c) is where momentum transfers more than this value results in reflectivity less than 'R_0'. This can be derived from Snell's law as discussed in Squires G. L. [10] and can be approximated as described by Klen K. [11] by;

$$Q_c[\text{Å}^{-1}] \approx 2\sqrt{\pi\rho b} \tag{6}$$

Where 'ρ' is the atomic density and 'b' is the mean value of the scattering length of the nuclei.

The slope in reflectivity as a function of momentum transfer is described by 'α' which occurs for momentum transfers greater than 'Q_c' up until the limit of $Q = mQ_c$. This 'm' value defines this limit, after which the supermirror cut-off 'W' defines the width of the curve.

The scattering vector is defined by;

$$\begin{aligned} Q[\text{Å}^{-1}] &= |\mathbf{k} - \mathbf{k}'| \\ &= \frac{m_n|\mathbf{v} - \mathbf{v}'|}{\hbar} \end{aligned} \tag{7}$$

Where '$\mathbf{k}$' is the wavevector of the incoming neutrons and '$\mathbf{k}'$' the wavevector of the scattered neutrons.

The scattering vector is discussed in more detail in the dissertation document (see Section 2.3.3, Appendix B). The underlying empirical formula describing this reflectivity as noted in the McStas components manual [9] (derived from experimental data) is given by;

$$R = \begin{cases} R_0 & \text{if } Q \leq Q_c \\ \frac{1}{2}R_0(1 - \tanh[\frac{(Q-mQ_c)}{W}])(1 - \alpha(Q - Q_c)) & \text{if } Q > Q_c \end{cases}$$

A diagram of the theoretical reflectivity for both a single and multilayer supermirror is shown in Fig.4 as obtained by Swissneutronics [12]. It is shown that the higher the m-coating, the more numerous the layers and the more that the reflectivity curve extends beyond the regime of total reflection, and as such, the larger the acceptance angle (i.e. neutrons incident at steeper angles are accepted).

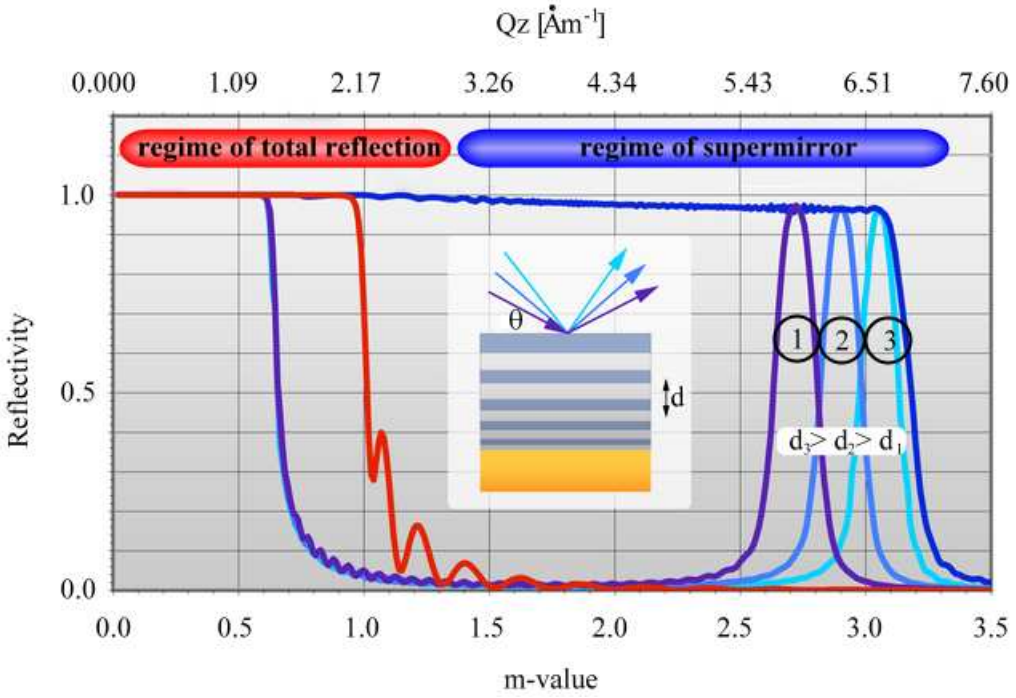

Figure 4: Theoretical supermirror reflectivity [12], where interlayer bragg scattering occurs due to multi-layers of different thicknesses as shown in label 1,2 and 3 causing the reflectivity curve to extend beyond the regime of total reflection.

4.3.4 Disk chopper component

This component as the name suggests describes an infinetly thin disk of radius R of a particular frequency of rotation. The disk can have slits of a chosen width and number through which the neutrons can pass. This component/device is often used as a velocity selector by trimming the incoming neutron beam and also in stopping frame overlap between successive pulses from the source as already described (see dissertation document, Section 3.2 Appendix B). A double disk choppers can be constructed by the use of two counter rotating single chopper components as shown in Fig.5 which are discussed by Well and Fredrikze [13] with expected triangular TOF curves after the DDC. This phase allows the changing of dynamic range by changing the open time. A PSC is similar in approach only that its purpose and therefore position differ. The PSC should be positioned as close to the moderator as possible where neutron energy distributions remain quite close together as shown in Fig.6, however, not too close where the chopper lifetime will be reduced. Its purpose being in shaping the moderator pulse as described by Demmel and Andersen [2].

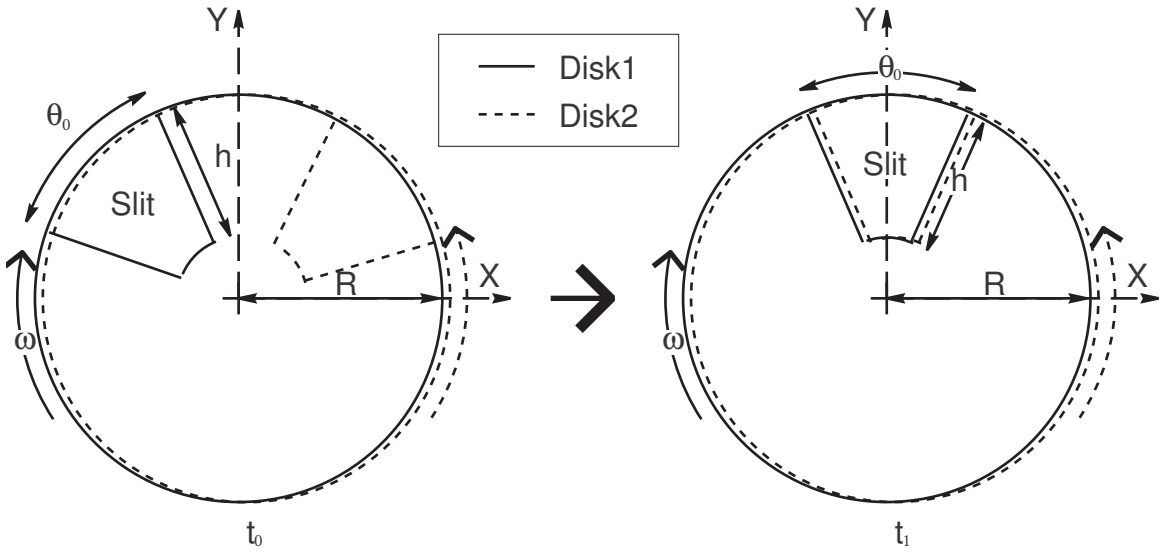

Figure 5: Counter-rotating double disk set-up shown for time 't_0' where slits do not overlap and 't_1', the time at which both slits overlap. Where 'ω' is the angular frequency, 'R' the disk radius, 'θ_0' the angular width of the slit(s) and 'h' the slit height.

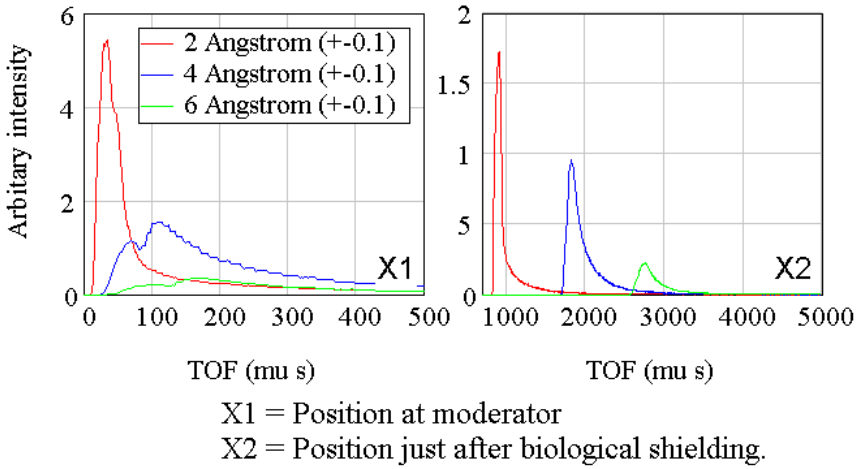

Figure 6: TOF distribution shown for different energy ranges. Clearly showing a separation of the faster neutrons (higher energy neutrons) from the slower.

4.4 Elliptic guides

Two elliptic types are considered in this investigation, one of which is that of the multi guide tapering component created by Schanzer C. et al. [8]. Another is a custom made elliptic offering complete control over guide geometry as described in Section 4.4.2.

4.4.1 Guide tapering component

The tapered guide by Schanzer C. et al. [8], has a symmetric elliptic taper which is one of many shapes offered by this component. The ellipse is defined by two focal distances together with entrance dimensions and guide length. The major and minor axis together with the end dimensions of the ellipse are then determined according to user defined focal distances. Limitations of this component mean that different m-coating distributions cannot be used and neither can be incorporating curvature to the geometry. As such, a custom made FORTRAN program for creating a guide from segments is required for complex geometries as described in Section 4.4.2.

4.4.2 Custom elliptically curved guide instrument

A program is necessary that allows the incorporation of user defined features to the guide including curvature, linear tapering and elliptic features in one or both dimensions of the guide.

The method to achieve this is by the writing of a FORTRAN program developed as part of this thesis to output an instrument file (see Appendix C).

An elliptic guide in two dimensions is described by different parameters. As such, an elliptic in the horizontal and vertical are independent. An illustration of such a guide is shown in Fig.7.

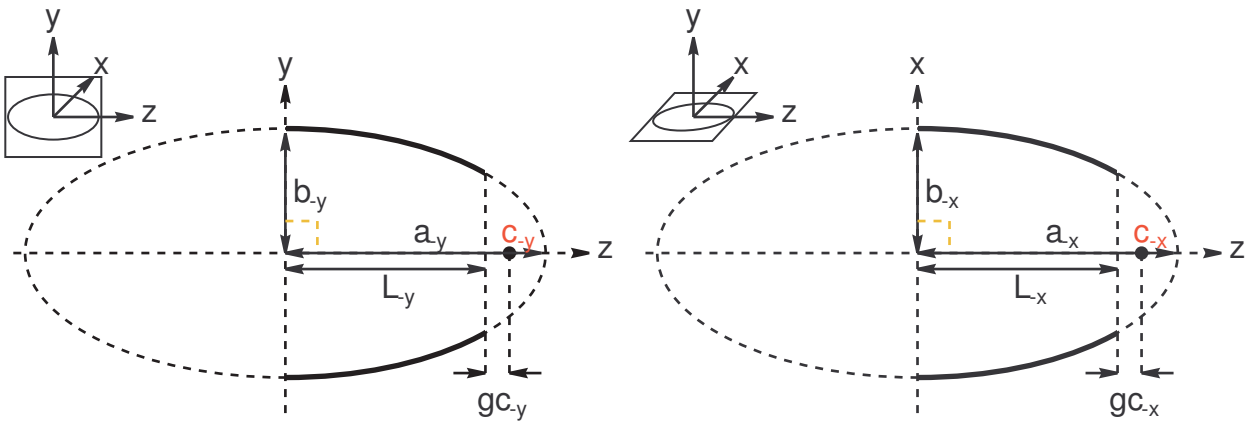

Figure 7: Illustration of a two dimensional elliptic guide along the 'z' axis, where 'c' denotes the foci point, 'gc' the distance from the guide exit to this foci, 'L' the elliptic length, 'b' the minor axis and 'a' the major axis of the ellipse.

Guide segments are larger towards the centre of the guide where the angle is low, but with smaller segments towards the end where the angle gets steeper. As such, an exponential distribution is used to describe the points along the guide as described by Klen K. [11];

$$z = \left[\exp\left(n\frac{\ln(\frac{L_T}{2.0}+1.0)}{(\frac{N}{2.0})}\right) - 1.0\right] \tag{8}$$

Where 'N' is the number of segments, 'L_T' the elliptic length and 'n' the segment number (0 to $(N\backslash 2)-1$). Similarly, the coating distribution is defined in the same way, and is given by;

$$m = \left[\exp\left(n\frac{\ln(L_T+1.0)}{(\frac{N}{2.0})}\right) - 1.0\right]\frac{(m2-m1)}{L_T} + m1 \tag{9}$$

Where '$m2$' and '$m1$' are the limits of the coating distribution resulting in a exponential distribution between '$m1$' and '$m2$'. Coating distributions then rounded to the nearest half integers.

A more detailed explanation of custom elliptic design and its derivation can be found on page 50, Appendix A.

5 Results and Discussion

Results presented are with some initially fixed parameters (i.e. constant throughout the results unless stated otherwise). The first of which is the distance from the very end of the guide to the sample environment at 35cm. The distance from the moderator to the guide entrance is also fixed at 1.698m. The straight guide in the biological section remains initially fixed at 4.544m unless stated otherwise.

5.1 Simple curved ballistic guide

Determination of instrument merit is key by comparison with other instruments. As such a set-up of the OSIRIS and IRIS[7] instrument parameters are simulated on a 90m long curved guide. Results through optimization of various guide types are then normalized according to that of IRIS parameter set-up in order to compare their factor of gain/loss.

IRIS consists of an m1 curved guide with a 1.8m m2 linear taper at the end. OSIRIS being similar only with an m2 curved guide and m3.6 linear taper. The design of these ballistic guides are shown in Fig.8. Both have dimensions $(4.3 \times 6.4)\text{cm}^2$ throughout. A detailed parameter set-up illustration is shown in Fig.51(AppendixA).

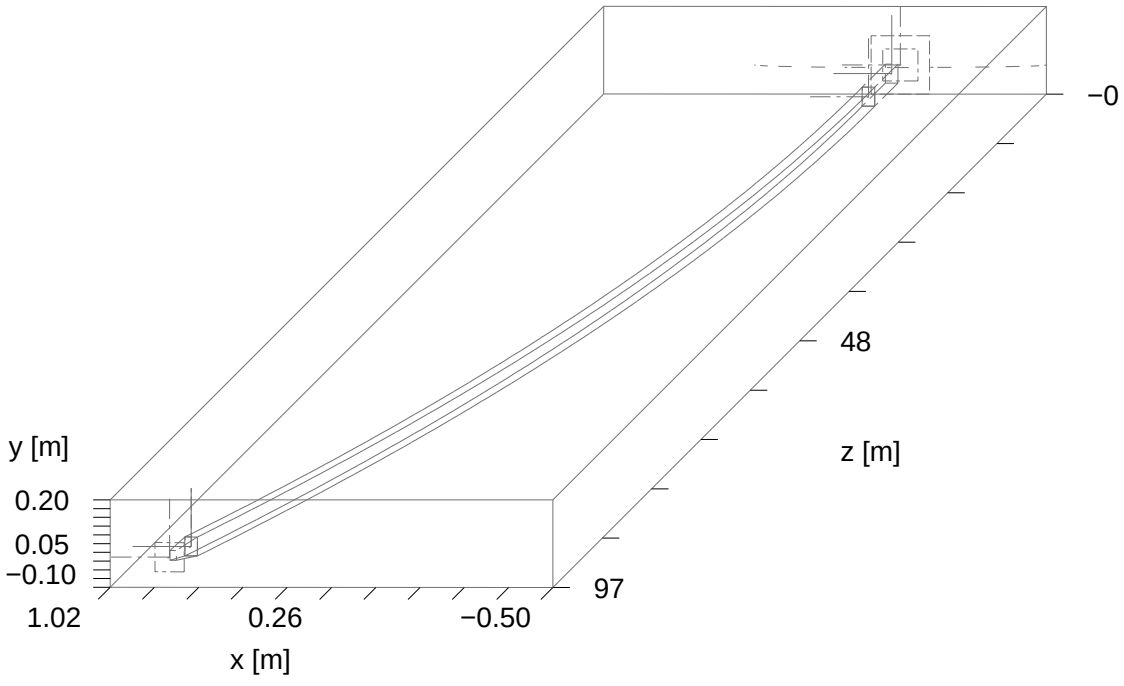

Figure 8: Design of the simple curved guide, OSIRIS and IRIS parameter set-up

Significant multiple peak formation is shown on the IRIS and OSIRIS divergence monitors as shown in Fig.9 and Fig.10 for IRIS and OSIRIS respectively. Each peak

corresponding to a segment of the guide with different m-coating. OSIRIS having an m2 guide together with an m3.6 linear taper means that the more divergent neutrons reach the end of the guide and these correspond to a maximum reflection associated with the coating. These then correspond to a third symmetric peak formation around 2° as shown in Fig.10. This indicates that allowing more divergent neutrons to reach the end of the guide fills up space, and as such produce a more homogeneous result at the sample position but at the cost of increasing divergence. PSD monitors at sample position of $(2 \times 3)\text{cm}^2$ of both set-ups indicate a rectangular shape resulting from the shape of the guide with the results for IRIS shown in Fig.11. Cross sections showing a gaussian spread after leaving the end of the guide (35cm after the guide exit) is shown in Fig.12. As such, gaussian fits are fitted using the least-squares Levenberg-Marquardt method for converging to the minima for the parameters describing the gaussian. These vertical and horizontal cuts through the PSD monitor respectively give a FWHM of $1.86 \pm 0.08\text{cm}, 2.88 \pm 0.16\text{cm}$ for IRIS and $1.94 \pm 0.07\text{cm}, 2.88 \pm 0.10\text{cm}$ for OSIRIS. These results indicate a $\times 1.5$ gain between the primary spectrometer of OSIRIS and IRIS in the 5-7Å range which agrees well with the data presented on the ISIS website [14].

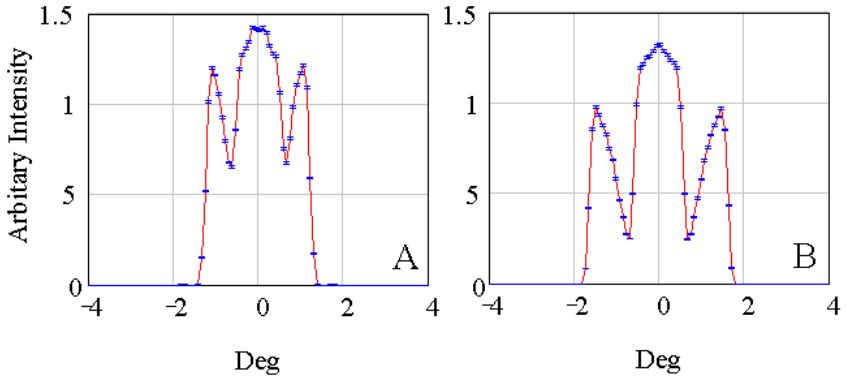

Figure 9: Divergence monitors for both horizontal(A) and vertical(B) at the sample position for the IRIS parameter set-up.

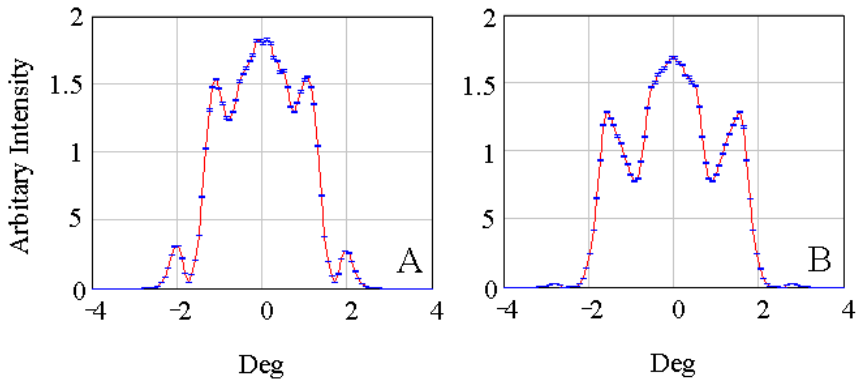

Figure 10: Divergence monitors for both horizontal(A) and vertical(B) at the sample position for the OSIRIS parameter set-up.

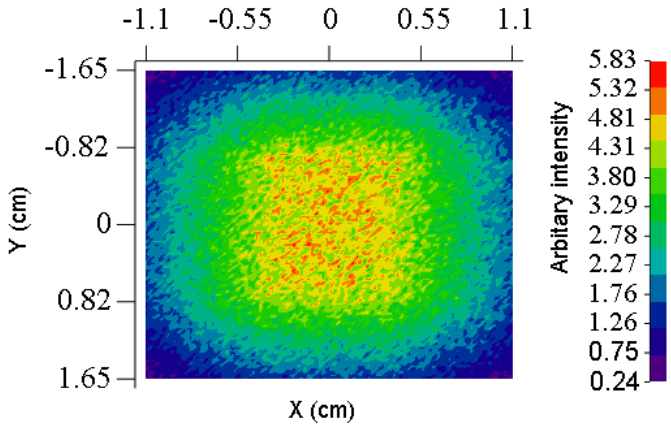

Figure 11: $(2 \times 3)\text{cm}^2$ PSD monitor at sample position for the IRIS parameter set-up.

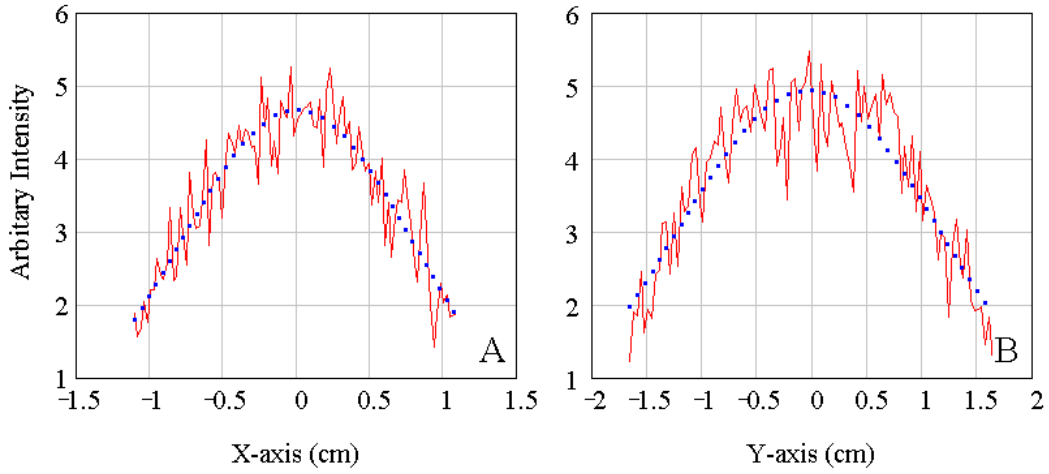

Figure 12: Horizontal(A) and vertical(B) slice through the IRIS $(2 \times 3)\text{cm}^2$ PSD at sample position.

5.2 Curved ballistic guide set-up

5.2.1 m2 Curved guide

Making a ballistic guide based on a similar design to the OSIRIS and IRIS instrument is first approached by placing a diverging and converging linear taper on the start and end of the guide respectively allowing the curved guide dimensions to be optimized. A diagram of the final set-up of the m2 and m3 standard curved guide is shown in Fig.18 (page 22). The curvature of the guide being important in stopping fast neutrons from reaching the sample position by removing direct line of sight to the source. Note that initially the coating of the entire guide to be m2. By varying the dimensions of the guide in a (2×3) scale and as such assuming independence between the horizontal and vertical, a maximum in intensity is found over the $(2 \times 3)\text{cm}^2$ sample area at guide dimensions of $(7.6 \times 11.4)\text{cm}^2$. The homogeneity of divergence worsens as the curved guide dimensions increase, for the reason that the angle of reflection becomes larger with the taper length remaining fixed. As such, optimization of the linear tapers are made. Acceptable taper lengths for different coatings are shown in Table 1, by merit of maximizing intensity but with consideration of homogeneity at the sample position. The results of each scan for different coatings are shown in Fig.13.

'm' Coating	$Taperlength(m)$
2	$\sim 7 - \mathbf{8}$
3	$\sim \mathbf{10} - 12$
4	$\sim 10 - \mathbf{12}$

Table 1: Acceptable taper lengths according to maximum intensity and suitable homogeneity over the $(2 \times 3)\text{cm}^2$ sample area. Note that the length highlighted in bold indicate the more suitable length according to homogeneity.

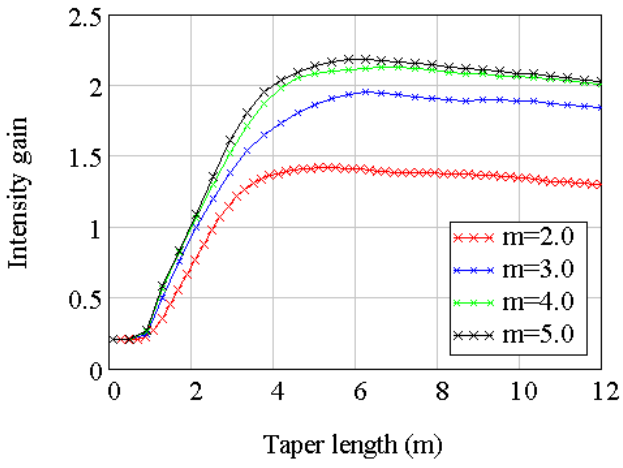

Figure 13: Integrated intensity over the $(2 \times 3)cm^2$ sample area show that the use of a linear taper with up to m5 shows some gain, though at the compromise of using longer taper lengths in order to take into account the homogeneity lost by the larger dimensioned curved guide. Very small taper lengths drop dramatically in intensity as the divergent neutrons are lost with the angle being too steep. Longer taper lengths improve homogeneity with more reflections causing space to fill-up by the end of the guide.

A linear taper of up to m4 is chosen with a length of 10m in order to achieve maximum intensity with the compromise of acceptable homogeneity at sample position. At this

length only $2.3 \pm 0.2\%$ gain is lost between the m4 and m5 taper coating (however with homogeneity being worse with m5 coating at this length as shown in Fig.14).

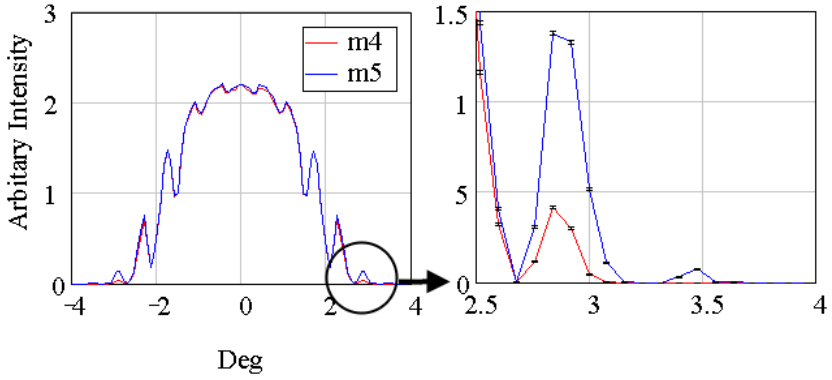

Figure 14: Increasing the coating shows an increase in intensity of the more divergent neutrons as shown above in the vertical divergence monitor.

Investigating how much m4 coating is necessary in order to achieve this gain, shows that only 2m of m4 is required with the rest being m3. This gives a total of 8m of m3 and 2m of m4. This is clearly shown in the illustration in Fig.15.

Looking at the diverging taper separately shows that no m4 coating is required as no gain being shown for any length of m4. The length of the diverging taper however indicates that intensity gain starts to level off at around 7m length as shown in Fig.16. However, the intensity does increase a further 2% by a length of 10m, together with an improvement in homogeneity and as such, this length is chosen as the most suitable. The results of which are shown in Fig.15.

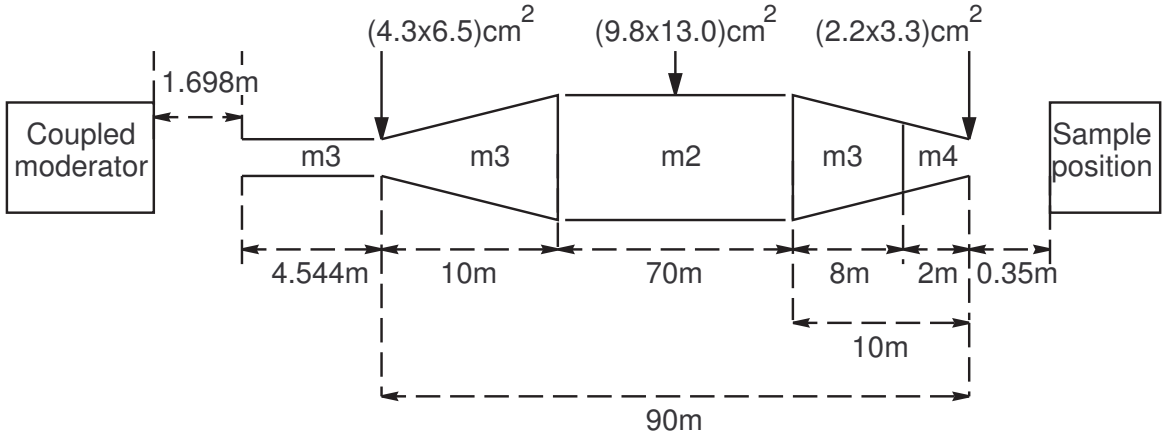

Figure 15: Parameter set-up of the optimized m2 ballistic curved guide.

Investigating the effect of changing the straight guide coating, shows that increasing to m3 results in some gain but marginal gains with more than m3. The increase in gain

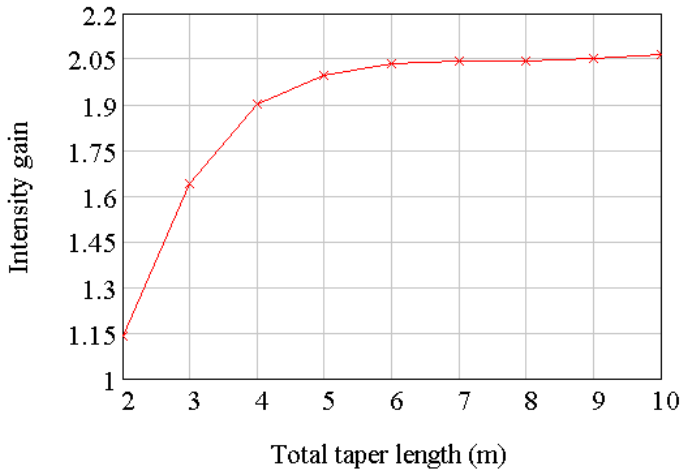

Figure 16: Changing the m3-coating diverging taper length shows clearly a leveling off at around 7m length, with some minor advantage to further increase this length to 10m. (Error is not shown as it is insignificant).

to m3 is 6% compared to m2 with the use of an m2 diverging taper. This gain however can be further increased yet another 3% by using an m3 coated diverging taper, to give a total increase in gain of 9% compared to a standard m2 straight section with an m2 diverging taper. As such, an m3 coated straight section together with an m3 diverging taper is the optimum set-up. This parameter set-up is shown clearly in the illustration on Fig.15.

These results show that the increased intensity by using an m3 straight section is lost using an m2 diverging taper, as these neutrons are too divergent to be reflected within an m2 diverging taper. Re-optimization of the guide dimensions independently is investigated having being likely to have shifted in its optimum set-up with different taper lengths chosen. The results of this investigation shown in Fig.17. From re-optimization of the curved dimensions independently, it is shown that optimum dimensions are $9.8 \pm 0.2cm \times 13.2 \pm 0.3cm$ which is not in the 2×3 scale. This indicates there to be some dependence between the horizontal and vertical parameters. Note that the intensity gains peak at the same dimensions over the $(1 \times 1)\text{cm}^2$ sample area.

Re-optimization of the straight section coating leads to similar results as found before re-optimization of the guide dimensions with marginal intensity gains above the use of m3. The final parameter set-up of the m2 ballistic curved guide is shown in Fig.15.

The final gain of the m2 curved guide compared to IRIS is $\times 2.3$ over the $(2 \times 3)\text{cm}^2$ sample area and $\times 2.1$ over the 1x1 sample area. The FWHM over the $(2 \times 3)\text{cm}^2$ PSD monitor at sample area is $2.40 \pm 0.07cm \times 3.30 \pm 0.10cm$.

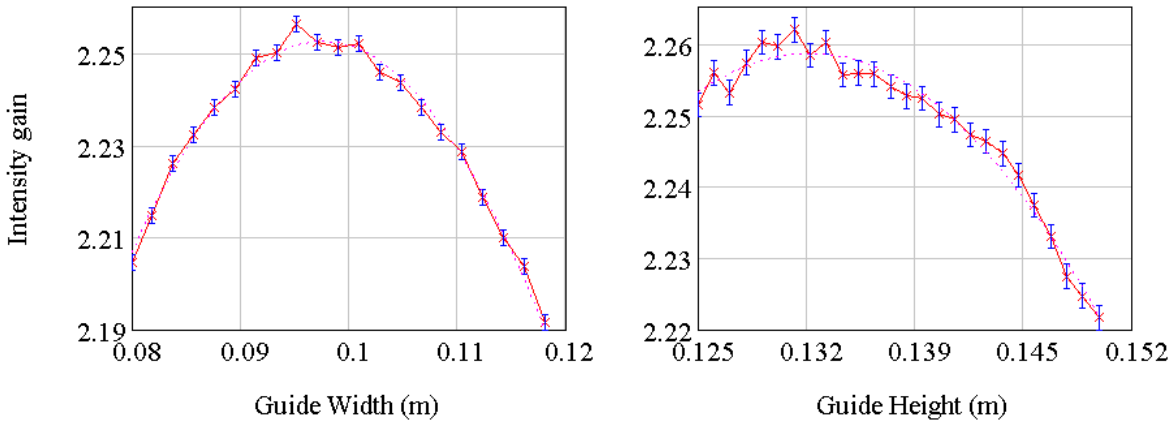

Figure 17: Changing curved guide width independent of height (height fixed at 13.0cm), changing curved guide height independent of width (width fixed at 10.0cm), data fitted with a gaussian.

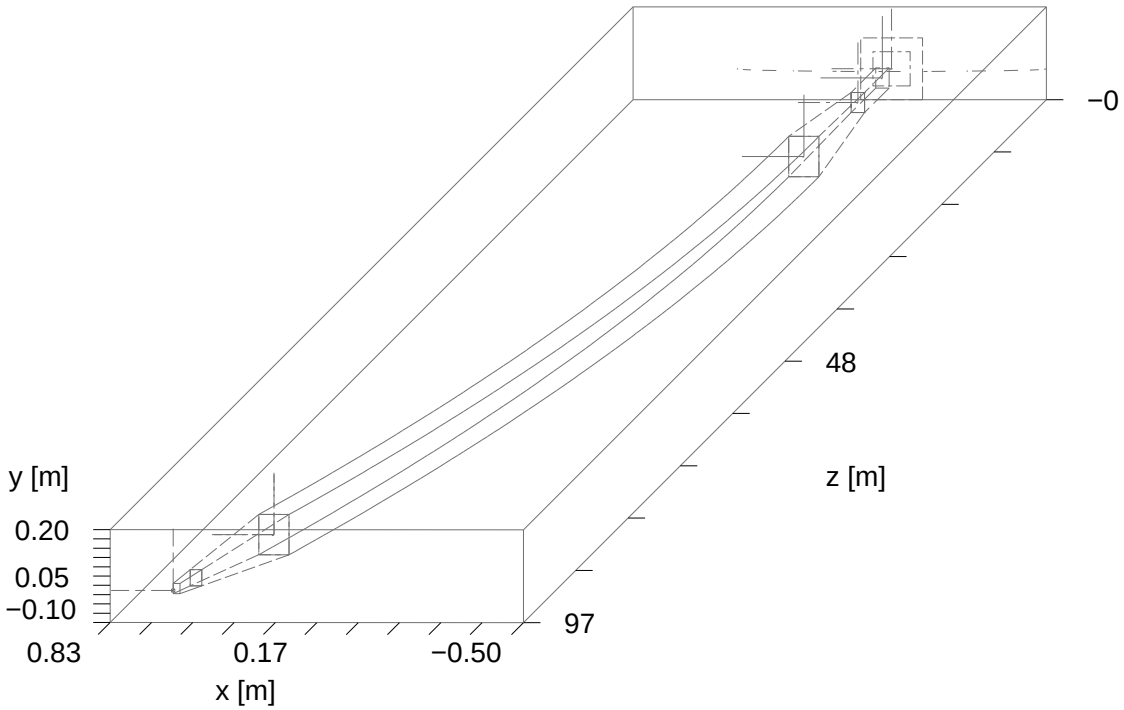

Figure 18: Design of the simple optimized curved guide.

5.2.2 m3 Curved guide

Investigation into using an m3 curved guide reveals that no gain is seen at the end of the guide without re-optimization of the taper sections. As such, investigating the coating of the converging taper is undertaken yet again, the results of which are shown in Fig.19.

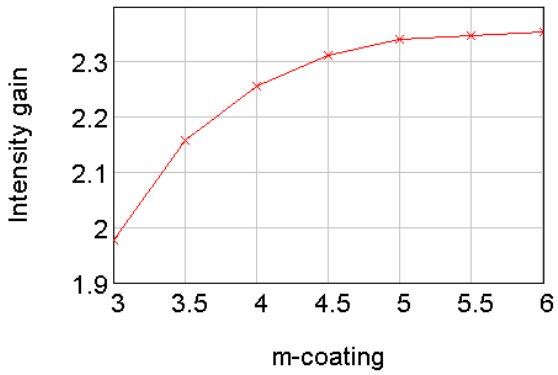

Figure 19: Changing the coating on the converging taper shows that there is some gain in intensity up to using m5 only with some marginal increase above this coating of $< 1\%$ together with the fact that these neutrons are increasingly more divergent and so will not be seen by a detector after hitting a sample.

From this scan, a converging taper with m5 coating is necessary to accept the increased divergent neutrons reaching the end of the guide from the use of an m3 coated curved guide.

Changing the length of m4 and m5 coating within the converging taper of total length 10m, reveals that only 1m of m5 is required to achieve the level of gain increase of this coating. Further investigation of changing the length of m3 and m4 coating with a fixed length of m5 (1m), reveals that only 1m of m4 is required. This means that a total of 8m of m3, 1m of m4 and 1m of m5 is required within the converging taper in order to accept the increased divergent neutrons from the m3 curved guide. This parameter set-up is shown clearly in Fig.20.

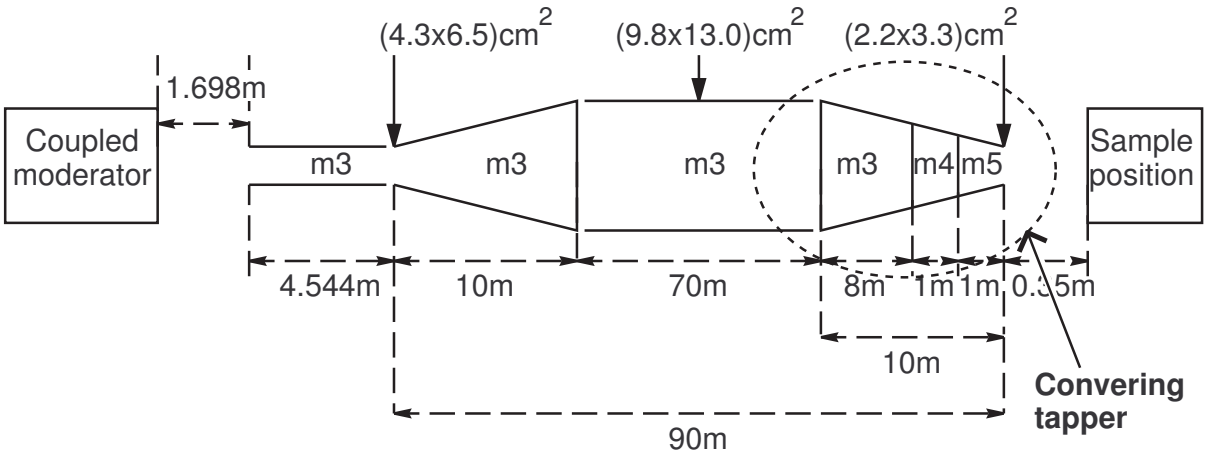

Figure 20: Parameter set-up of the custom optimized m3 curved guide.

Optimum dimensions of the curved guide remain unchanged with peak positions the same over the $(2\times3)\text{cm}^2$ as-well as the $(1\times1)\text{cm}^2$ sample area. The straight guide coating still shows insignificant gain above m3 coating.

The final results of an m3 optimized guide show an increase of 8% gain over the $(2 \times 3)\text{cm}^2$ sample area and a 5% increase in gain over the $(1 \times 1)\text{cm}^2$ sample area compared to the m2 curved guide. The FWHM over the $(2 \times 3)\text{cm}^2$ sample area is $2.66 \pm 0.09cm \times 3.18 \pm 0.10cm$. The final results of this set-up for the $(2 \times 3)\text{cm}^2$ PSD sample area are shown in Fig.21. Results show that this small increase in intensity between an m2 and m3 custom curved guide, is also the more divergent neutrons making homogeneity worse as shown in Fig.22.

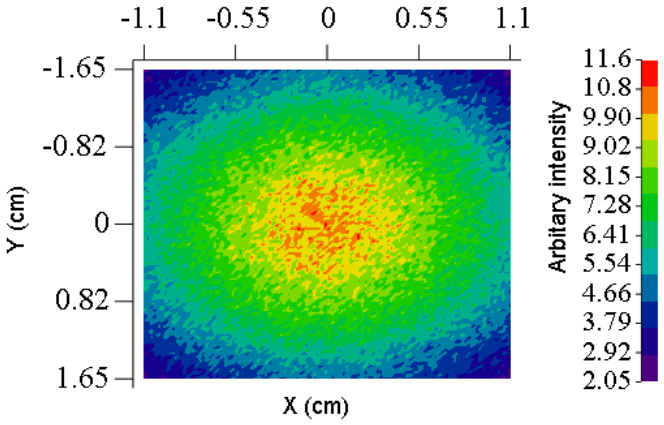

Figure 21: $(2 \times 3)\text{cm}^2$ PSD monitor at sample position for the m3 curved guide.

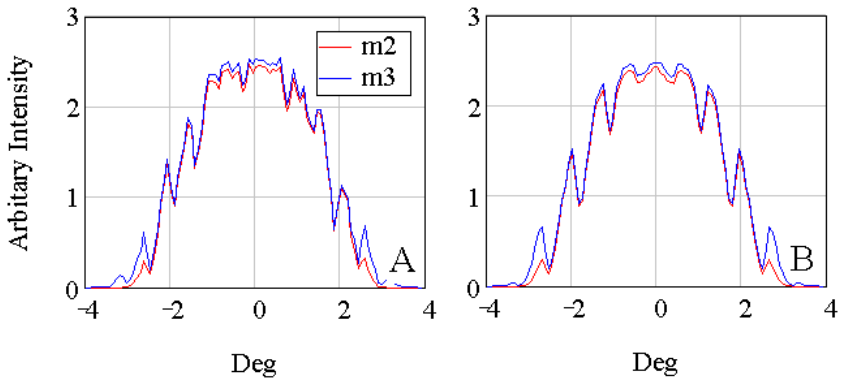

Figure 22: Divergence monitors for both horizontal(A) and vertical(B) at the sample position for both m2 and m3 curved ballistic guide. Note, error is insignificant for this plot.

5.3 Elliptically tapered curved guide

The use of an elliptically tapered curved guide is a logical step between an elliptic full and a standard curved guide. The starting set-up is an m2 curved guide from Section 5.2 only with elliptical tapering of m3-coating at the end in both horizontal and vertical planes. The first step in its optimization being in the scanning of its length. Note that the straight section in the biological shielding remains with a coating of m3 due to the increase in neutrons entering the curved section as described in Section 5.2. The starting dimensions of the elliptic taper fixed at $(9.8 \times 13.0)cm^2$ according to the results found for the curved ballistic set-up Fig.5.2.1. The results of the length optimization of the elliptic taper are shown in Fig.23.

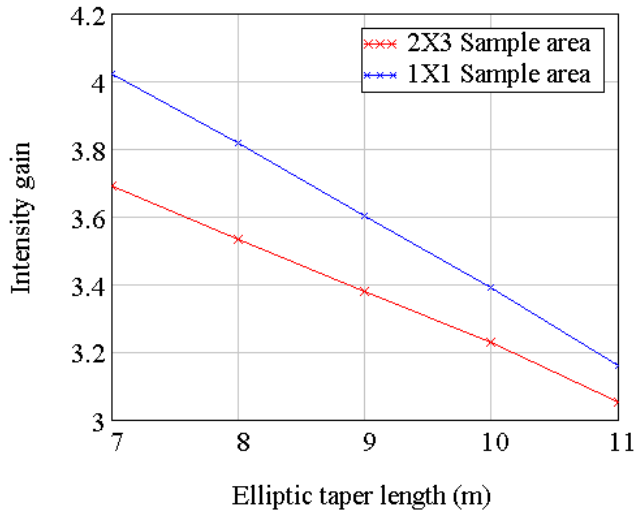

Figure 23: Results of changing the elliptically tapered curved guide length. Improved intensity gain with decreasing taper length however at the cost of homogeneity. Note, error is insignificant for this plot.

The optimized elliptic taper length chosen is 8m for the reason of both intensity gain and homogeneity though this length is dependant on application. The homogeneity becomes increasingly worse with shorter elliptic taper length as shown in Fig.24.

Investigation of the coating of the taper shows marginal gain over using m5 as shown in Fig.25.

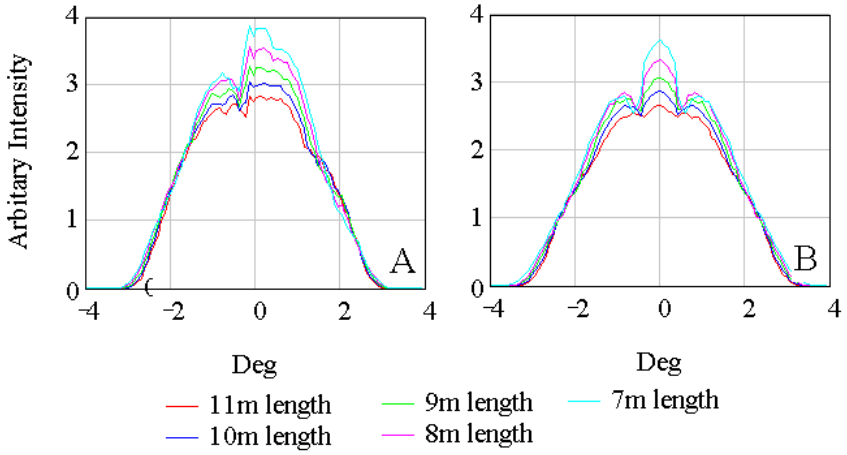

Figure 24: Comparison shown between the homogeneity of the different lengths of elliptically tapered curved guide for both horizontal(A) and vertical(B). Note, error is insignificant for this plot.

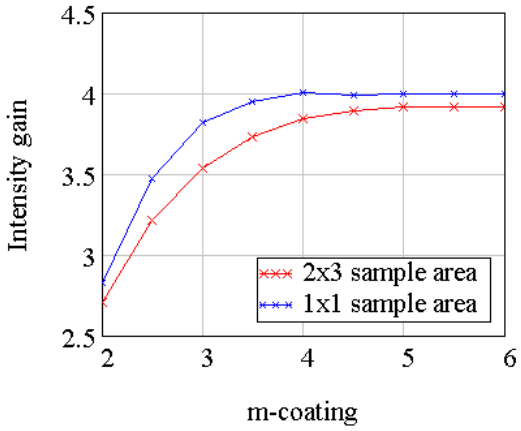

Figure 25: Changing the coating of an elliptically tapered m2 curved guide. Note, that error is not shown as it is insignificant.

A diagram of this set-up is shown in Fig.26.

Increasing the curved guide coating shows similar results as with the m2 curved guide, with only a $\times 0.9 \pm 0.3\%$ difference in gain between an m6-coated and m5-coated elliptically tapered guide, but with $\times 1.9 \pm 0.3\%$ drop between the use of m5 to m4. For this reason, an m-coating distribution between m3 and m5 is used in the elliptic taper.

Increasing the curved guide to m3 results in marginal gain. The divergence of the final m3 curved elliptically tapered guide is shown in Fig.28, where asymmetry of the curve in the horizontal is due to the curvature of the guide with neutrons reflecting off the one side of the guide.

The final gain of the m3 curved guide with elliptically tapered end is $\times 3.9$ over the $(2 \times 3)\text{cm}^2$ sample area and $\times 4.0$ over the $(1 \times 1)\text{cm}^2$, with a FWHM of 2.4 ± 0.17cm for horizontal, 2.52 ± 0.15cm and vertical cut through the $(2 \times 3)\text{cm}^2$ PSD. The intensity gain from an m2 curved guide to the m3 curved guide (both elliptically tapered) being insignificant as within error. A parameter illustration is shown in Fig.29.

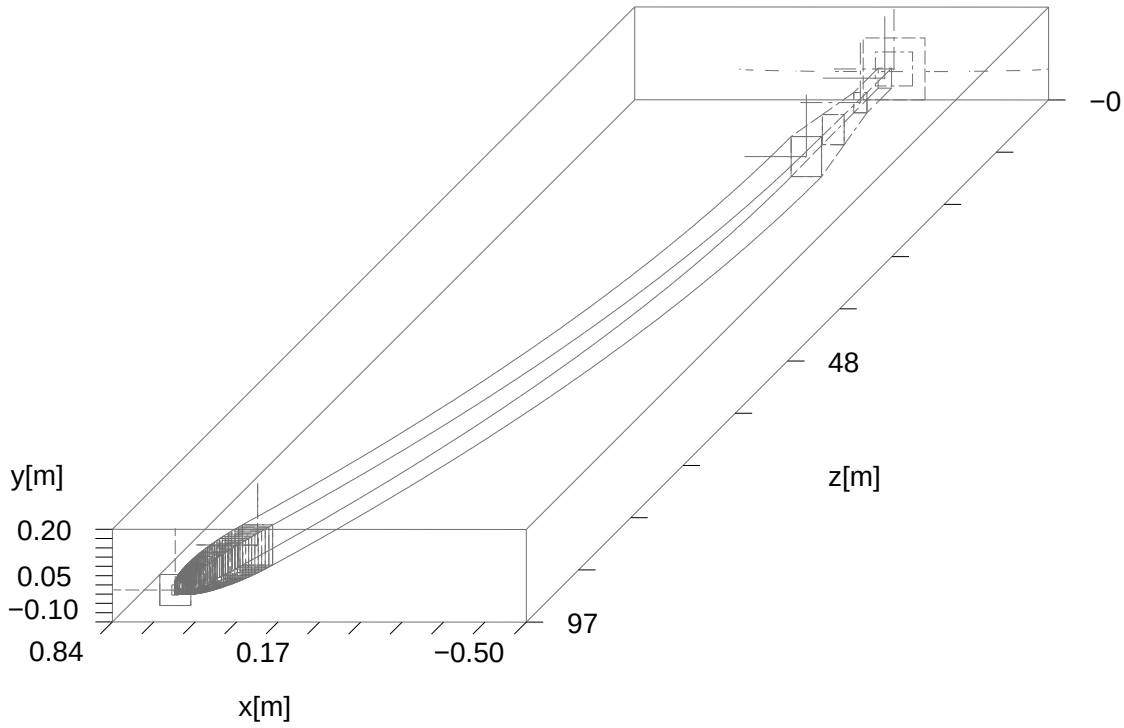

Figure 26: Elliptically tapered curved guide.

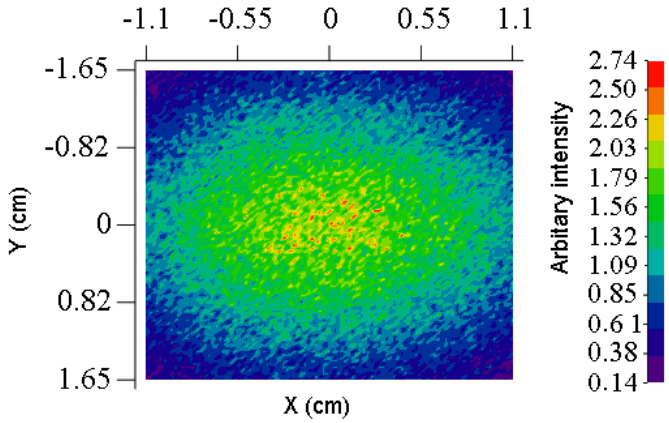

Figure 27: $(2 \times 3)\mathrm{cm}^2 cm^2$ PSD monitor at sample position for the elliptically tapered guide.

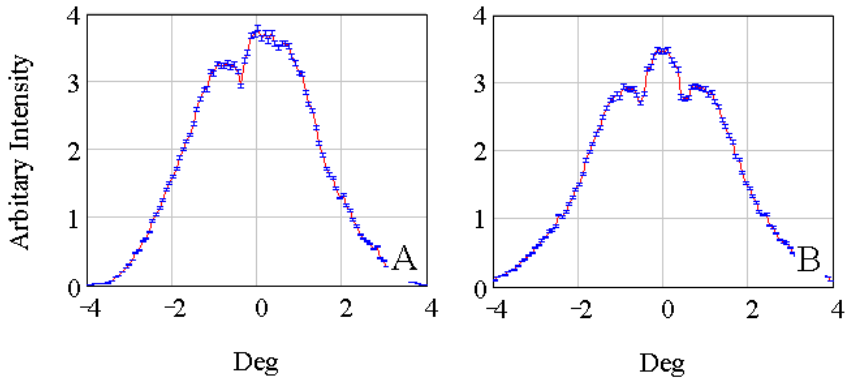

Figure 28: Horizontal(A) and vertical(B) divergence monitors at the sample position for the elliptically tapered guide.

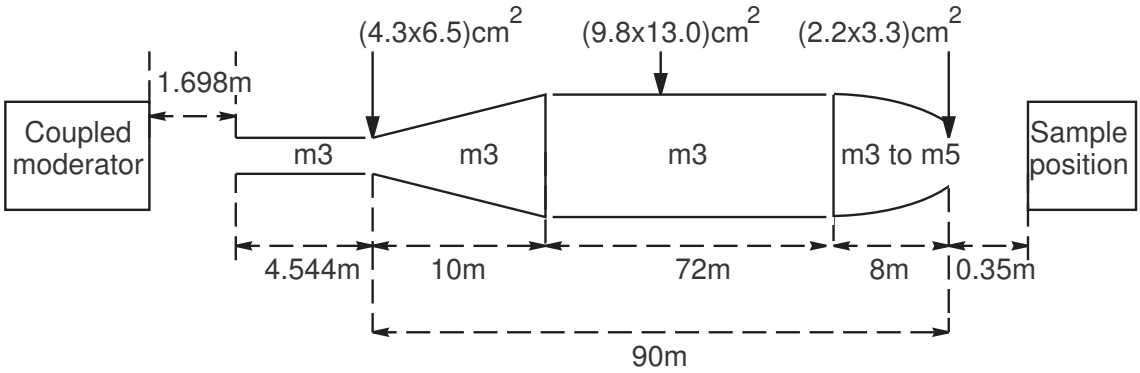

Figure 29: Parameter set-up of the elliptically tapered curved guide.

5.4 Full vertically elliptic curved guide

The next step in guide set-up is the investigation into combining a vertically elliptic guide but still however blocking highly energetic neutrons by the use of a horizontally curved guide.

5.4.1 Symmetric elliptic guide

The set-up of a symmetric vertically elliptic guide by the use of the custom made elliptic instrument as described in Section 4.4.2, in principle should offer the best results in maximizing guide transmission from the biological shielding. A diagram of the set-up is shown in Fig.30. A graphical plot of the guide dimensions are shown in Fig.31. Note that the vertical first foci distance is defined in Section 5.5. Horizontally an elliptic taper of 8m length is again chosen at the end of the guide as described by Section 5.3.

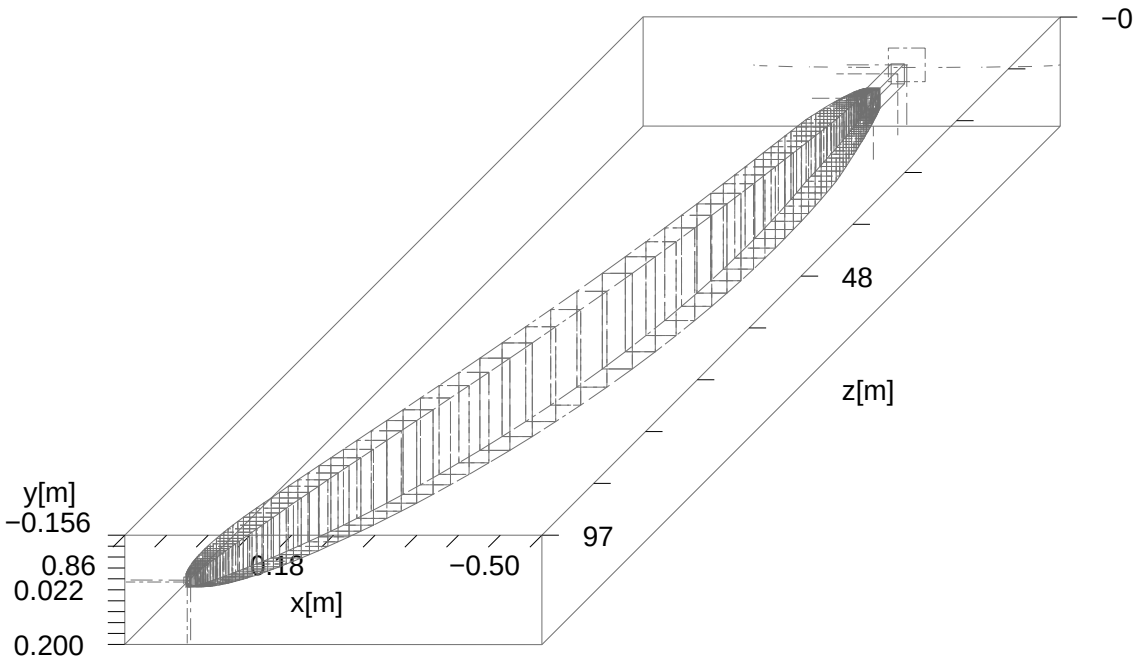

Figure 30: Design of the vertically symmetric elliptic guide.

Most parameters of the guide are fixed as the entrance dimensions are set by the straight guide section. Optimization of the guide coating is shown in Fig.32.

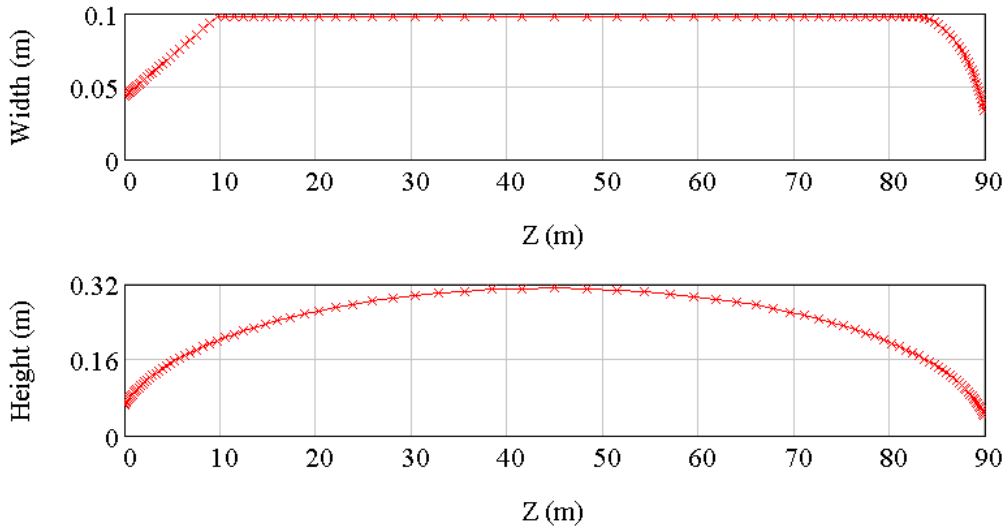

Figure 31: Graphical plot of the guide dimensions as a function of distance along the z-axis.

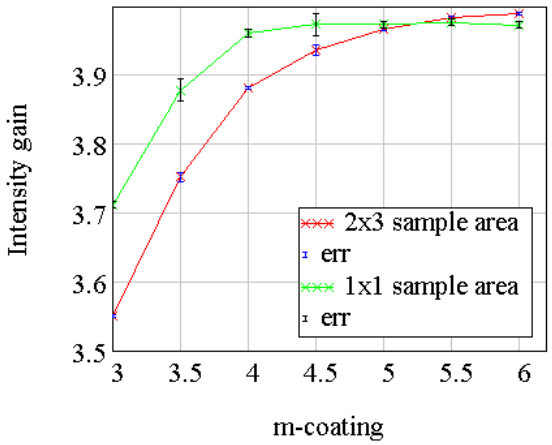

Figure 32: Changing total coating of the guide shows marginal intensity gain over the $(2\times3)\text{cm}^2$ sample area for coatings above m5.5, however coatings above m4 show marginal gain over the $(1 \times 1)\text{cm}^2$ sample area.

The final results of the optimized symmetrically elliptical guide in the vertical and curved in the horizontal, show that the optimized design reaches maximum dimensions of 32 ± 1cm in the vertical, with a gain of $\times 4.0$ over the $(2 \times 3)\text{cm}^2$ sample area and $\times 4.0$ over the $(1 \times 1)\text{cm}^2$. For constructional reasons elliptic designs with reduced height are investigated (i.e. non-symmetric).

5.4.2 Non-symmetric elliptic guide

As expected from results on symmetric elliptic design, the larger the vertical minor axis becomes and the closer it is to the symmetric design, the better the intensity becomes for the non-symmetric design at the end of the guide. One with a vertical minor axis of 10cm and another with 7.5cm.

As in the case for the symmetric design, the entrance dimensions remain fixed, however the centre position of the double ellipse (meeting point) is a variable in which to define symmetry between the two ellipses. The theory behind the elliptic (non-symmetric) is described in Section 4.4 only with considering two ellipses together, and defining the point at which the two meet for a fixed guide length of 90m.

Results of the optimum symmetry of the two are shown in Fig.33. Note that corresponding vertical first focal distances for the different lengths follow a linear relationship with changing symmetry. Note that coating of the following set-ups initially take exponential distributions between m3 and m5.

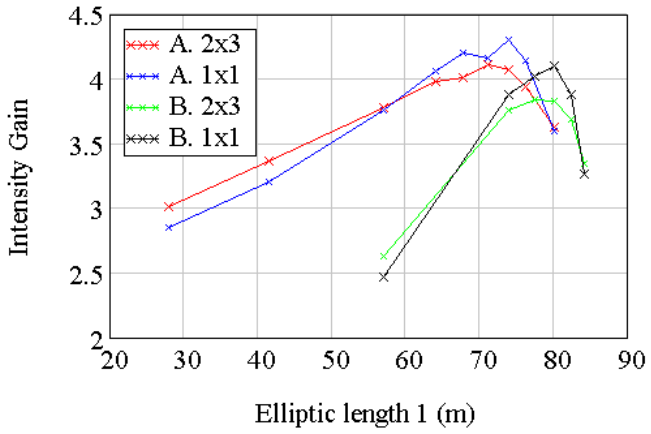

Figure 33: Plot of symmetry change by varying the two elliptic lengths, where 'A.' is the 0.1cm minor axis set-up and 'B.' is the 0.075 minor axis set-up. Changing the guide symmetry shows that a reduction in intensity gain with decreasing symmetry shown. Note that errors are not shown as they are small. Deviations from the curve result from the lost homogeneity over the $(2\times3)\text{cm}^2$ monitor.

The resulting set-up dimensions can be shown clearly in Fig.34

The final gain of this set-up with m3 to m5.5 coating distribution with a minor axis of 10cm over a $(2\times3)\text{cm}^2$ sample area is $\times4.1$, and $\times4.2$ over the $(1\times1)\text{cm}^2$ sample area. This set-up is $13.0\pm0.3\%$ higher in gain over the $(2\times3)\text{cm}^2$ area in comparison to the symmetric design, even with a lower overall transmission compared to the symmetric. The increase in gain over the $(1\times1)\text{cm}^2$ sample area in comparison to the symmetric design is 19.9 ± 0.7 gain. Decreasing the minor axis from 0.1m to 0.075m results in a loss of $17.4\pm0.3\%$ over the $(2\times3)\text{cm}^2$ sample area and a $2.1\pm0.2\%$ loss over the $(1\times1)\text{cm}^2$ sample area. This indicates the non-symmetric approach to be advantageous is focusing the neutrons over the sample area. Homogeneity is similar to that of the symmetric elliptic however, slight deviations from the optimum set-up results in a significant decrease in homogeneity. This divergence of the non-symmetric elliptic is shown in Fig.35.

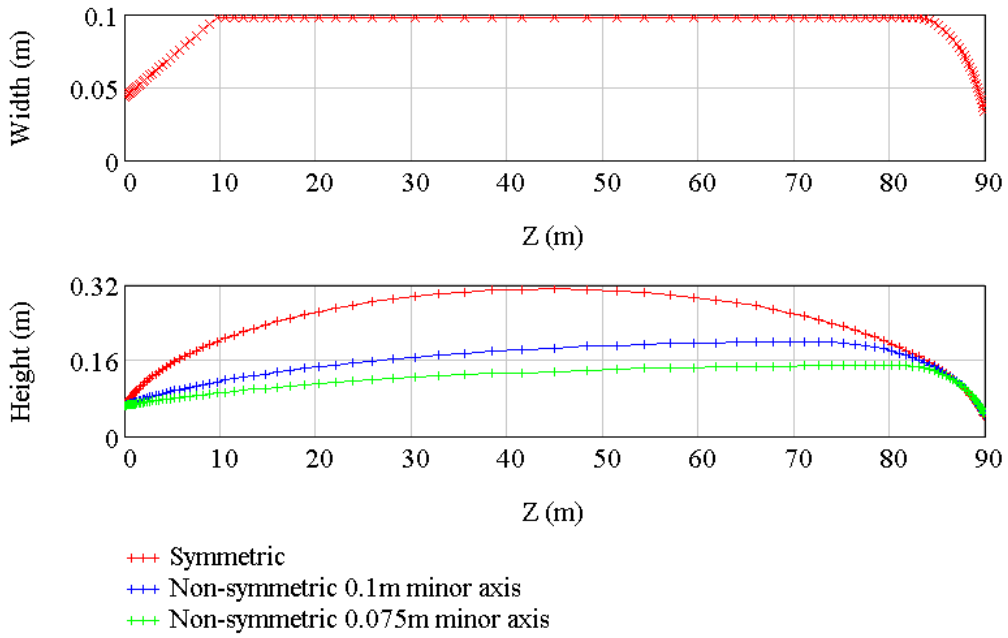

Figure 34: Graphical plot of the guide dimensions as a function of distance along the z-axis showing the non-symmetry of the double elliptic in the vertical in comparison to the symmetric set-up.

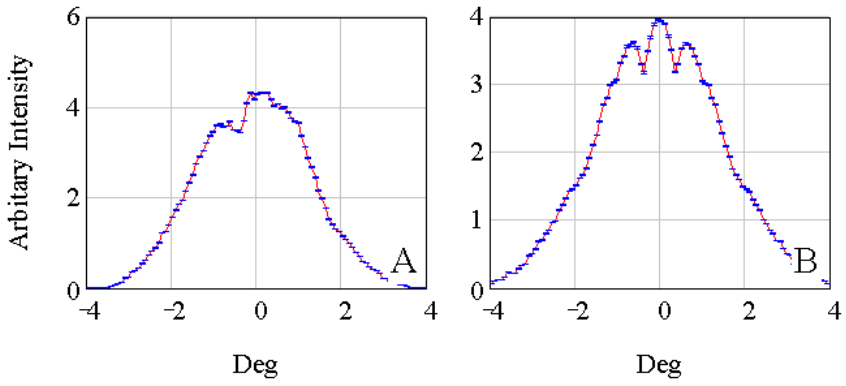

Figure 35: Divergence monitors for both horizontal(A) and vertical(B) at the sample position for the m3 to m5.5 distributed vertically non-symmetric elliptic guide (10cm minor axis).

5.5 Full elliptic guides

Mathematically, the best shape to deliver the greatest number of neutrons from one point to another is the elliptic shape as this offers the least number of reflections to occur. Focal distances can be shifted and as such, this design makes a very keen option for instrument design. In the present case, the full elliptic in both horizontal and vertical planes, there is a direct line of sight, and as such, fast neutrons are allowed to reach the sample position. This means that the background signal is high and intensity at the sample position is larger than should be expected from a curved guide. The following set-up's however allow the investigation of biological shield modification.

Optimizing the full symmetric elliptic entails using the *guide_tapering* component as described in Section 4.4.

5.5.1 Full elliptic from moderator

The full elliptic from the moderator consists of two focal distances. The second still remains fixed as determined by the fixed distance from guide exit to the sample area (35cm). The first foci distance however in both horizontal and vertical requires optimization as it cannot be accurately defined analytically. The horizontal and vertical entrance dimensions of an m2 full elliptic guide are changed independently in order to determine the optimum entrance dimensions to the guide together with both horizontal and vertical first foci distances. The entrance dimensions (and therefore, major and minor axis of the ellipse) however are coupled to the focal distances, and so changing the foci distances effect the optimum entrance dimensions found. For this reason, the full elliptic from moderator is only a semi-optimized design but does indicate there to be considerable gain in biological shielding modification. Set-up of the semi-optimized design for the full elliptic is shown in Fig.36. Chosen semi-optimized parameters for the full elliptic from moderator are shown in Table 2.

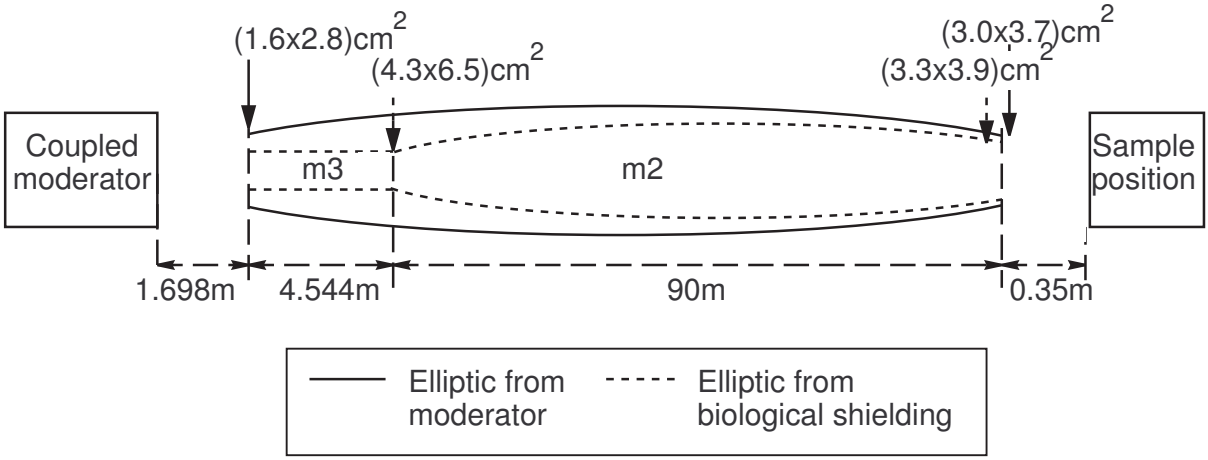

Figure 36: Parameter set-up of both the full elliptic from the moderator and the full elliptic from biological shielding.

The results of an m3 full elliptic from the moderator are a gain of $\times 12.0$ over the $(2\times 3)\text{cm}^2$ sample area and $\times 13.1$ over the 1x1 with a FWHM of $1.94\pm 0.02\times 2.54\pm 0.04$. This significant gain indicating the advantage of biological shield modification rather than standard straight section set-up from the moderator. It is also shown that the optimum minor axis of the ellipse in both horizontal and vertical are rather large, and this being due to the total length of the guide with the required focal distances.

Investigation of m-coating shows that this increases the divergence significantly at the end of the guide as shown in Fig.37. The circular profile can be shown from elliptic geometry in Fig.38. Investigation into a full elliptic from the biological shielding is made in order to determine how much of a gain is possible from biological shield modification as described in Section 5.5.2.

Optimized area ($cm \times cm$)	Entrance ($cm \times cm$)	Exit ($cm \times cm$)
2×3	1.6×2.8	3.0×3.7
Minor axis ($cm \times cm$)	Foci1 Horizontal (m)	Foci1 Vertical (m)
24.6×30.5	0.1	0.2

Table 2: Final parameters for the full elliptic from moderator.

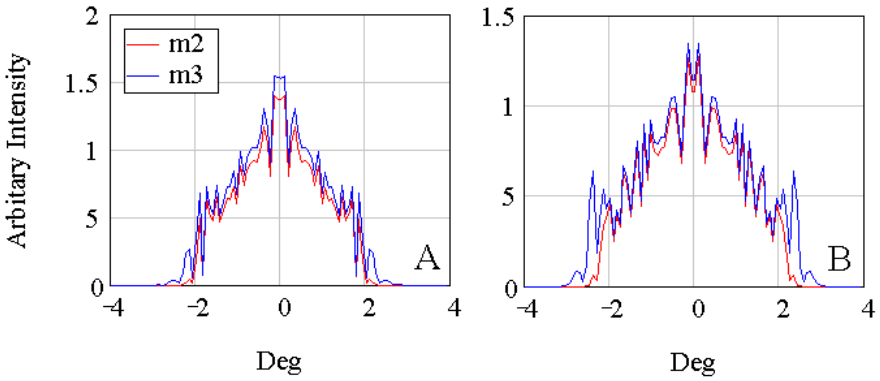

Figure 37: Comparison between divergence of a full elliptic m2 coated and an m3 coated from moderator to sample. Note that error is not shown as it is insignificant.

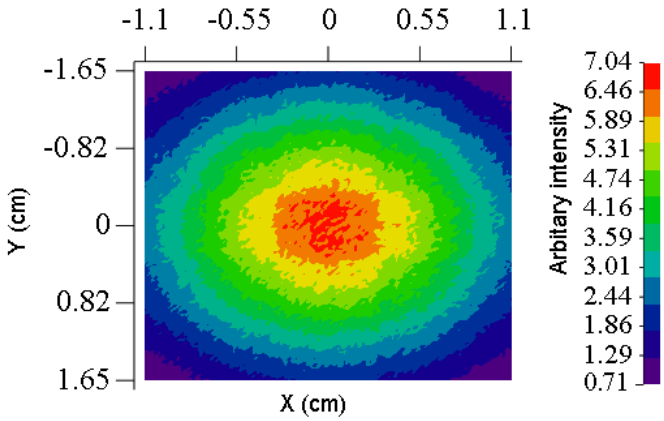

Figure 38: $(2 \times 3)\text{cm}^2$ PSD monitor at sample position for the m3 coated elliptic from moderator showing a circular profile in both horizontal and vertical axis.

5.5.2 Full elliptic from biological shielding

Set-up of a full elliptic from biological shielding as shown in Fig.36 allows the determination of the effect of biological shielding modification.

The entrance dimensions of a full elliptic from the straight section are fixed at $(4.3 \times 6.5)cm^2$ which is the dimensions of the straight section in the biological shielding. Horizontal and vertical focal distances however require optimization. Optimized results of the full elliptic from the biological shielding is shown in Table 3.

The gain of the optimized m3 full elliptic guide form the biological shielding is $\times 3.7$ over the $(2 \times 3)\text{cm}^2$ sample area and $\times 3.5$ over the $(1 \times 1)\text{cm}^2$ sample area. This shows that there is a significant drop in intensity by the use of the straight guide section ($\times 8.3$ gain difference), but with still rather large minor axis dimensions of these two set-ups. The full elliptic from the moderator also has to accommodate the pulse shaping chopper and as such a comparison between both symmetric and non-symmetric elliptical guides from the biological shield is necessary. Non-symmetric full elliptic set-ups from the moderator are however difficult to define manually as many parameters are coupled. As such, an automated optimization routine for finding minima is suggested as the approach for further investigation into this possibility.

Optimized area $(cm \times cm)$	Entrance $(cm \times cm)$	Exit $(cm \times cm)$
2×3	4.3×6.5	3.3×3.9
Minor axis $(cm \times cm)$	Foci1 Horizontal (m)	Foci1 Vertical (m)
13.3×15.6	0.6	1.0

Table 3: Final parameters for the full elliptic from the biological shielding.

5.6 Overview of chopper consideration

Chopper implementation is based on obtaining a specific width from the incoming moderator pulse. The width requirements being around $50\mu s$ to up the possibility of $200\mu s$ pulse width.

The position of the PSC in the set-up of the guide is set, having to be as close to the moderator as possible (where neutron velocity distributions are very close together) for maximizing the dynamic range as described by Demmel F. and Andersen K.H. [2]. As such, it is positioned straight after the biological shielding (6.242m after the moderator). From this position for the PSC with a pulse width of $50\mu s$, analytical calculations as discussed by Demmel F. [2], indicate an elastic energy resolution of around $2.4\mu eV$ with a width of $200\mu s$, a resolution of $6.5\mu eV$ and a dynamic range of around $250\mu s - 300\mu s$ to be expected.

The pulse shaping chopper consists of a double counter-rotating disk set-up as described in Section 4.3.3. An analytical chopper window of 10.8 deg is required to obtain a suitable pulse width, however a window of 10 deg is used to obtain a pulse width of $50.0 \pm 0.5\mu s$ according to its FWHM as shown in Fig.39. The resulting width of the lambda distribution is then shown in Fig.40.

It can be clearly shown that the dynamic range is heavily restricted with a narrow energy range as shown in Fig.40. This width is $0.286 \pm 0.004\mathring{A}$ at 20% its maximum intensity and $0.220 \pm 0.004\mathring{A}$ at 30%.

Changing the time at which the PSC is open, is investigated and shown in Fig.41 where intensity decreases with increasing phase time as expected from the intensity lambda distribution from the moderator. These curves normalized are shown in Fig.42 according to both position and wavelength, indicating the FWHM not to change as a function of this change in phase. These results show that the limiting factor of the energy distribution from the PSC is due to its position (far enough away from the moderator at which neutron energies are already separated). Results showing this separation of neutron energy in time at this position are shown in Fig43. For this reason, an arrival time of 6.4Å is chosen giving a maximum peak around 6.27Å which is the wavelength accepted by the analyser Si(111) in the secondary spectrometer. This limits the width of the energy distribution and so the dynamic range at this resolution.

Results for the 100Hz set-up for obtaining lower resolution but higher dynamic range and intensity is shown in Fig.44 resulting in a pulse FWHM of $153.0 \pm 0.1\mu s$ and for the lambda distribution in Fig.45, $0.349 \pm 0.004\mathring{A}$ at 20% intensity and $0.266 \pm 0.004\mathring{A}$ at 30%.

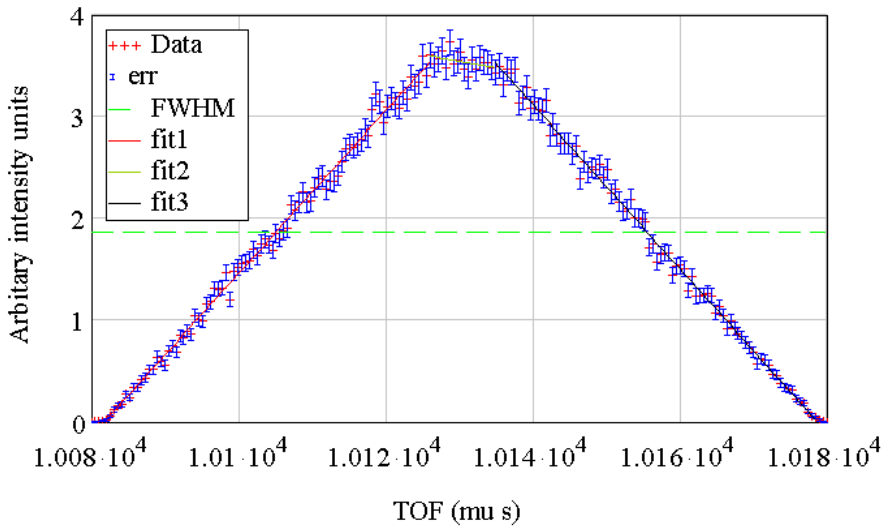

Figure 39: The TOF plot after the 300Hz PSC is fitted with a trapezium. This shape is characteristic of the double chopper opening over the curved guide dimensions with flattened peak being the time when both chopper slits overlap over the guide dimensions for a length of time. The centre of the slit corresponds to an arc length 4.6cm.

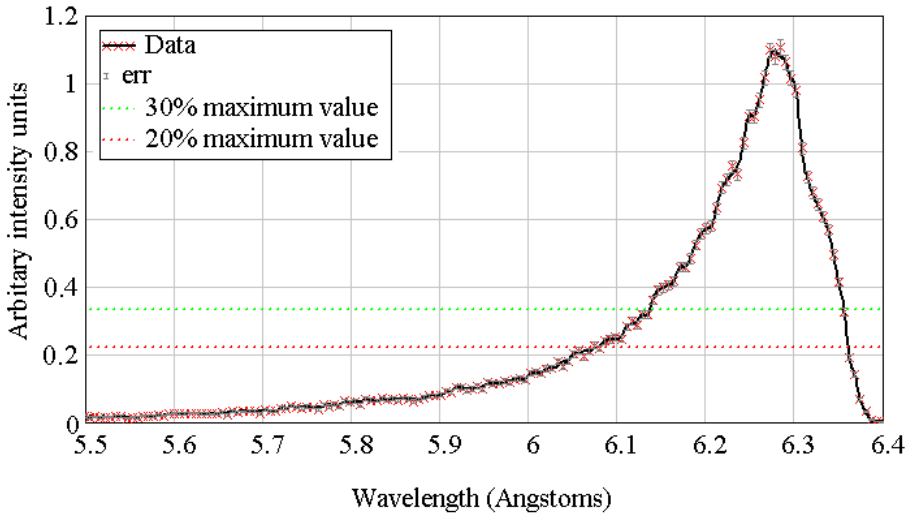

Figure 40: Lambda distribution after PSC(300Hz) position.

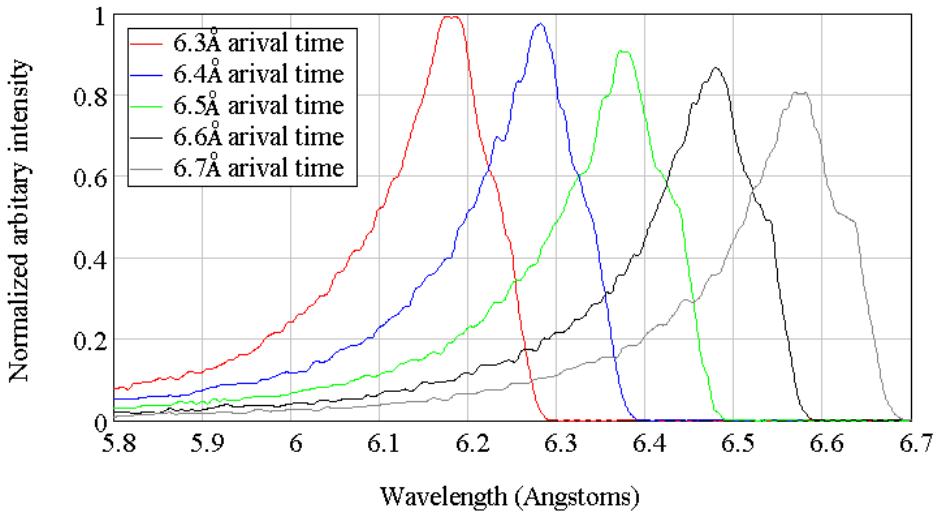

Figure 41: Energy distribution of incoming rays for different PSC phase time (based on wavelength arrival time at full opening). Note that the error is small and considered insignificant for this plot.

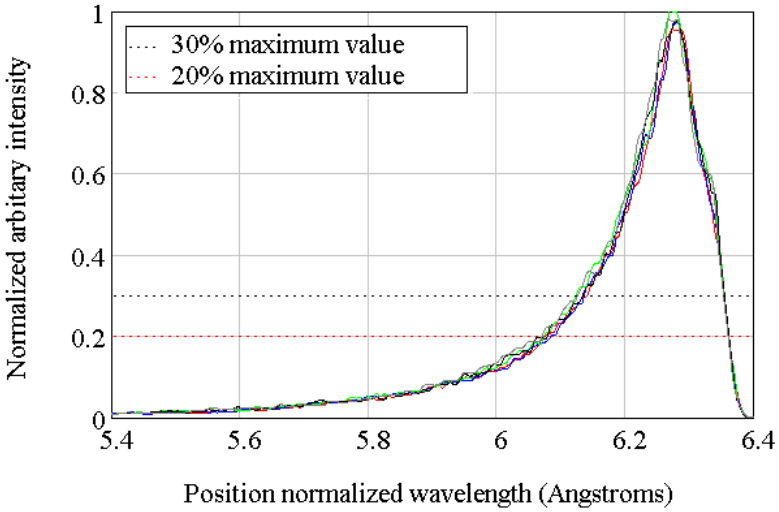

Figure 42: Distribution curves from Fig.41 normalized in both intensity and wavelength position. Note that error is small and considered insignificant for this illustrative plot. The results show a FWHM that doesnt change for different times of the PSC.

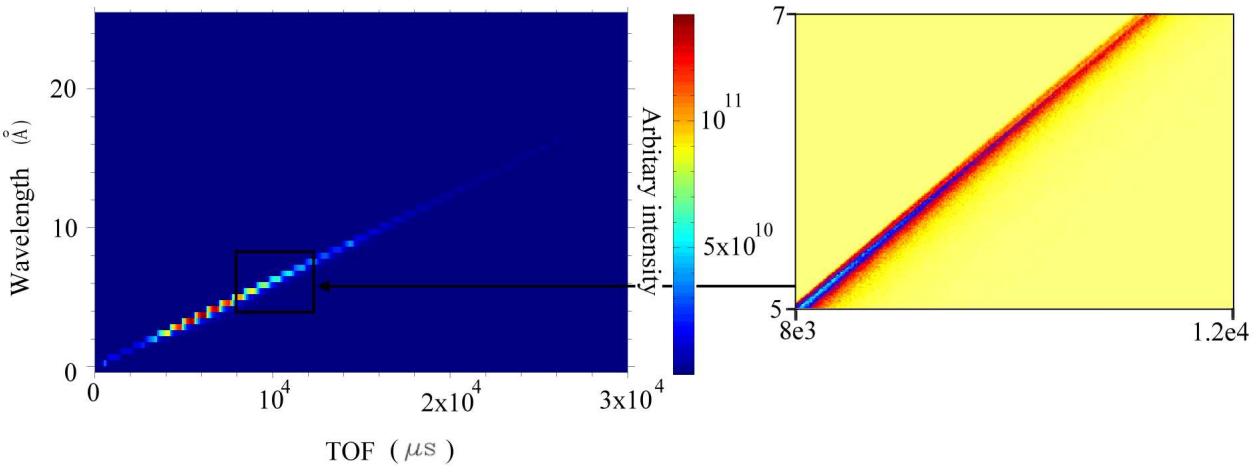

Figure 43: TOF-Lambda distribution just before the PSC position clearly shows a separation in neutron energies with a clear cut-off at any point over a particular wavelength.

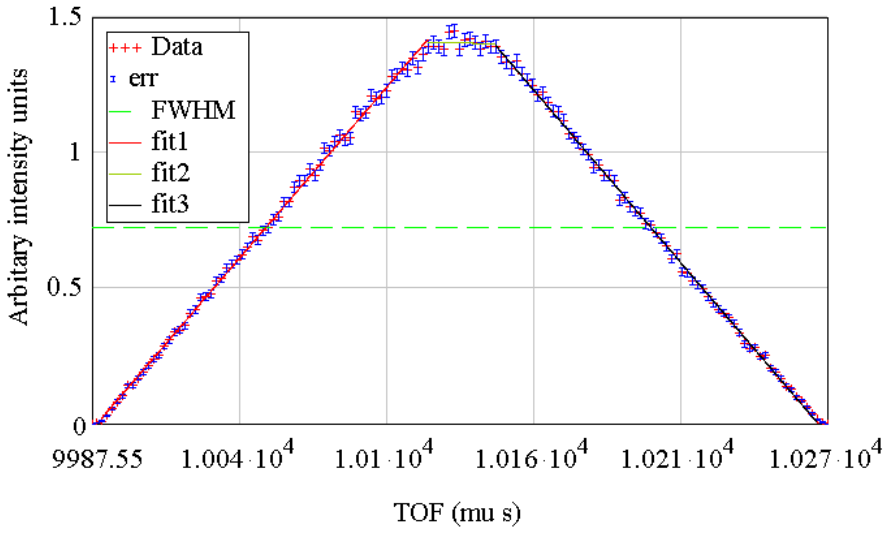

Figure 44: TOF plot after the 100Hz PSC position. The TOF plot is again fitted with a trapezium.

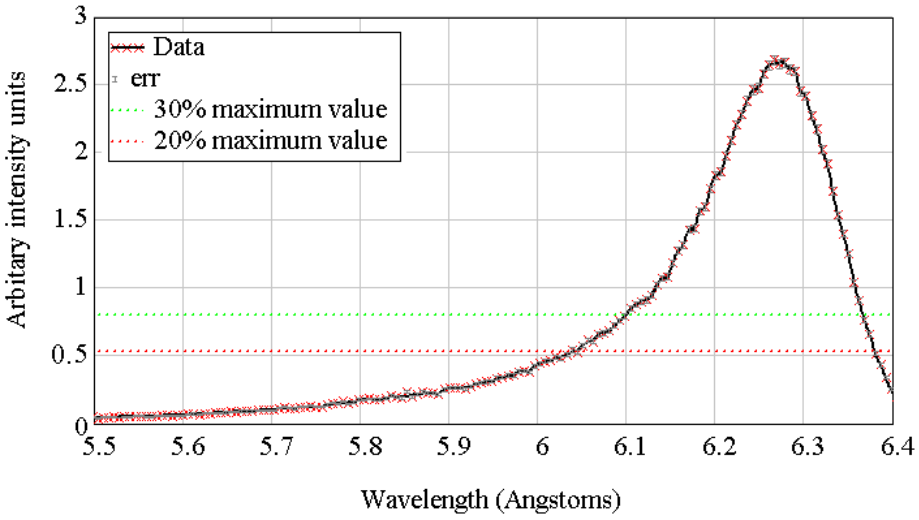

Figure 45: Lambda distribution after PSC(100Hz) position.

Other choppers are required for the elimination of frame overlap between successive moderator pulses and also from unwanted pulses from the PSC. Chopper windows of the double disk chopper and first overlap chopper are not optimized for the required set-up. They are set-up according to achieving a single pulse at the sample position from the six pulses from the PSC in $50\mu s$ mode. It should be noted that a second overlap chopper is likely to be required in order to stop frame overlap between successive moderator pulses. Set-up of these choppers according to typical expected positions are shown in Fig.46.

The basis in which chopper windows are set, are according to making the fully opening time match the pulse width at the specified position. Maximizing the energy distribution being made for this chopper set-up overview, is set for a width that covers down to 5% the maximum intensity of the energy distribution for the lower resolution set-up ($150\mu s$). The resulting fully opening times of the DDC are then $500\mu s$ and $1000\mu s$ for the overlap chopper. It should be noted however, that the chosen width of these choppers is for investigating the effect of a single pulse from the PSC rather than a set-up based upon specific quasi-elastic/inelastic requirements.

Results show that this simple chopper set-up results in a single pulse at the sample position. This is demonstrated by Fig.47. Final results at sample position show a width of $0.22 \pm 0.01 \mu eV$ at 20% intensity and $0.17 \pm 0.01 \mu eV$ at 30% intensity for the $150\mu s$ PSC set-up. With the PSC at $50\mu s$ set-up a width of $0.19 \pm 0.01 \mu eV$ at 20% intensity and $0.14 \pm 0.01 \mu eV$ at 30% intensity is observed. This is shown in Fig.48.

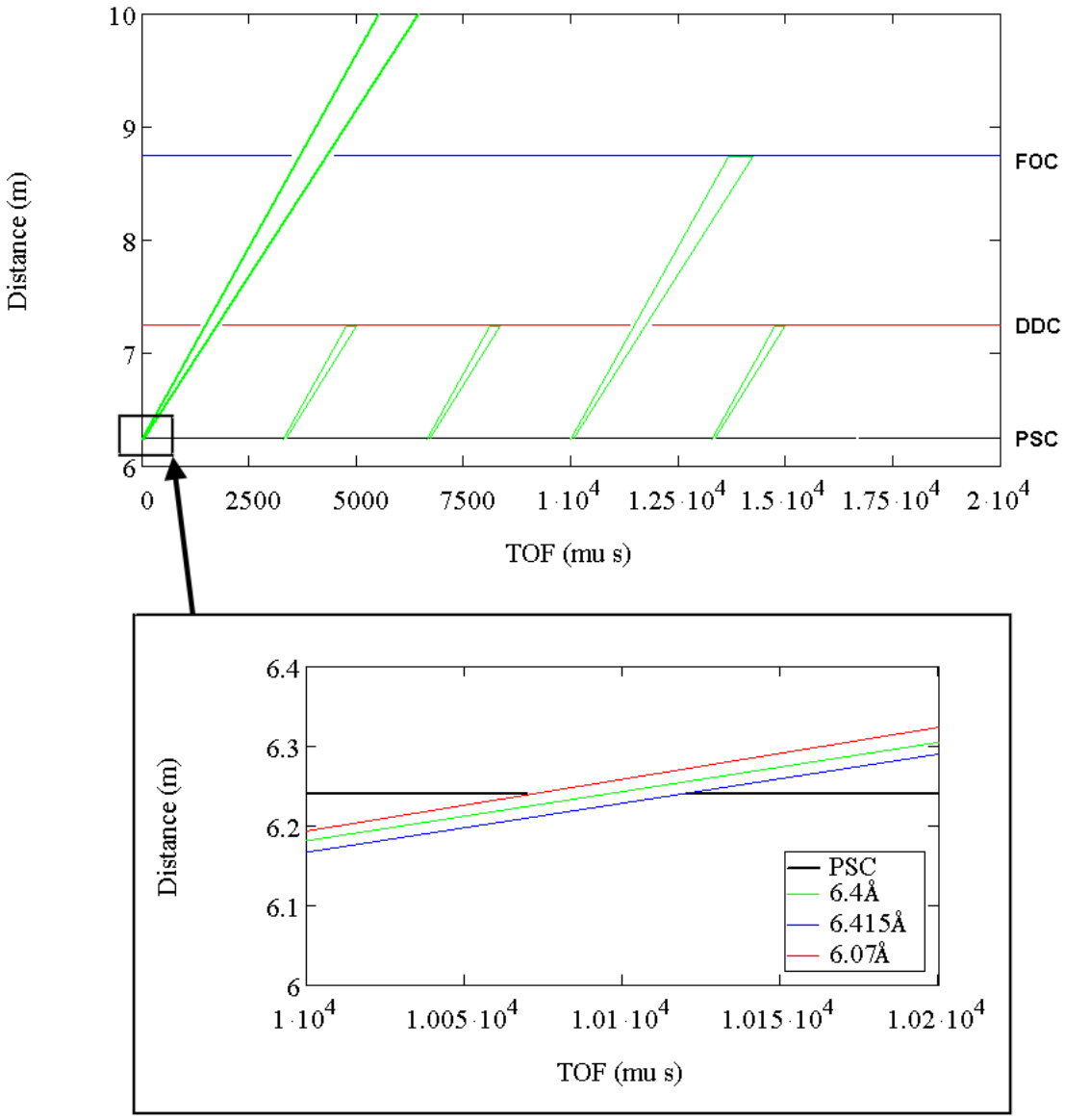

Figure 46: Chopper window and position set-up with pulse shaping chopper (300Hz) showing slower wavelength neutron rays entering at the extreme end of the moderator pulse (500μs, where intensity has dropped to around 10%). Here neutrons as fast as 6.07$\AA$ are shown to enter the PSC which corresponds fairly well with simulated results shown in Fig.40, where this wavelength corresponds to intesity of around $10-20\%$ of its maximum value.

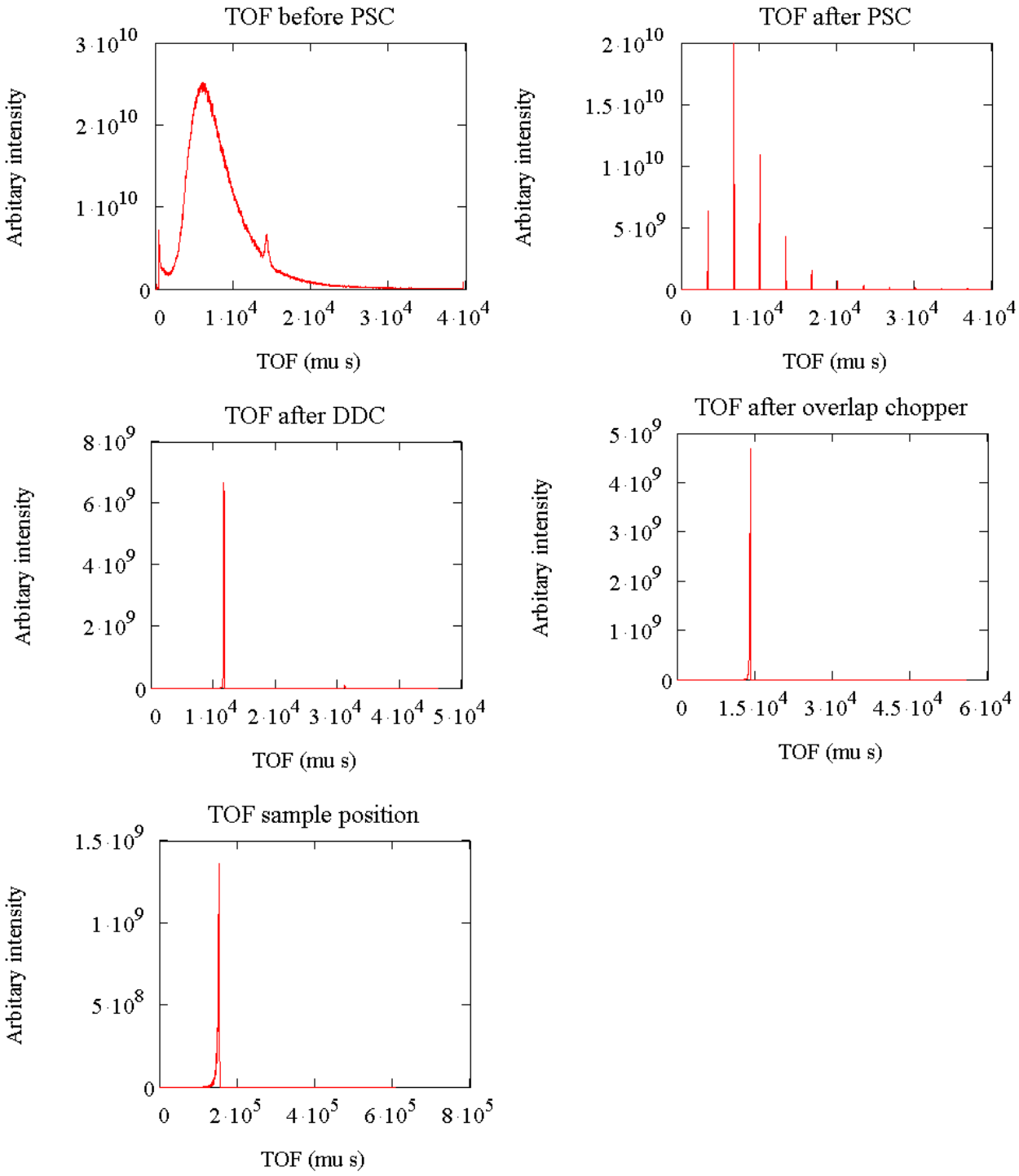

Figure 47: TOF plots at various points showing the resulting single peak at sample position (from a single moderator pulse).

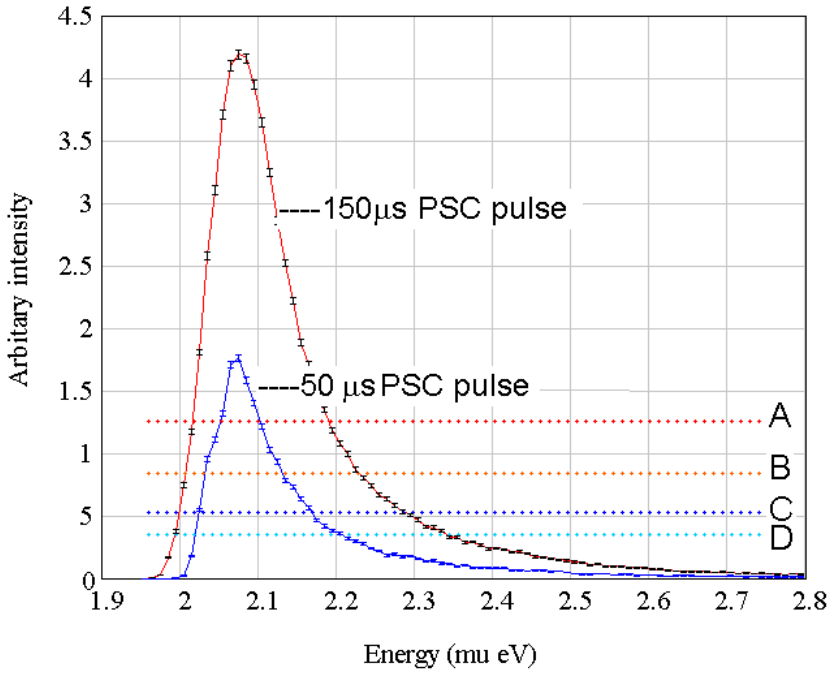

Figure 48: Energy plot at sample position for both PSC set-ups where 'A' and 'B' indicate the 30% and 20% drop from maximum intensity respectively for the 150μs PSC pulse. Similarly 'C' and 'D' indicate that for the 50μs PSC pulse.

6 Conclusion

A comparison between the various guide designs, indicate a dimensionally optimized simple curved guide set-up to be of a considerable higher gain to the standard elliptic. However it is also shown that the gain can yet significantly increase by the use of an elliptically tapered guide set-up as shown in Section 5.3 with a gain of $\times 3.9$ over the $(2 \times 3)\text{cm}^2$ sample area. Some further gain is also shown in the non-symmetric vertically elliptic design, horizontally curved, with a gain of $\times 4.1$. A comparison between the various set-ups are shown in Fig.49.

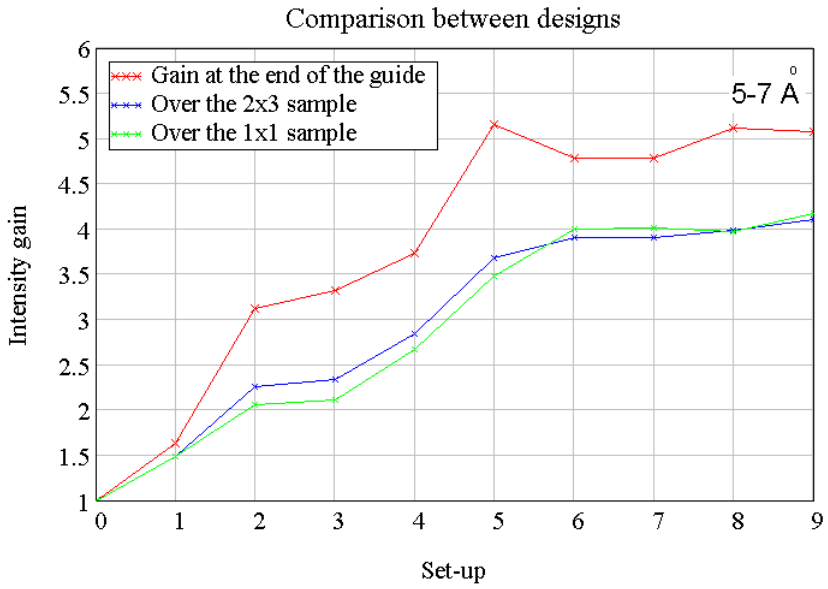

Figure 49: Comparison between various optimized guide set-ups. Note that results here are normalized according to the IRIS parameter set-up. The set-up key is shown in table4. Note, error to be insignificant.

The comparison between the various set-ups shown in Fig.49 indicates the limit of intensity gain or transmission with no change made to the biological shielding. However, results as described in Section 5.5 show that a further gain in excess of $\times 3$ may be possible with further investigation of elliptic guides from the moderator position rather than the biological shielding where transmission through an m3 bioshield alone is indicated to be 50%. A symmetric or non-symmetric elliptic from the moderator is a logical step in further investigation (i.e. with modification to the biological shielding). Such a set-up has no defined parameters, and as such makes it a difficult set-up for manual optimization with a number of parameters being coupled. Automated parameter optimization routines are suggested as a more suitable technique for finding minima in such a set-up.

A comparison between the transmission of each guide is shown in Fig.50.

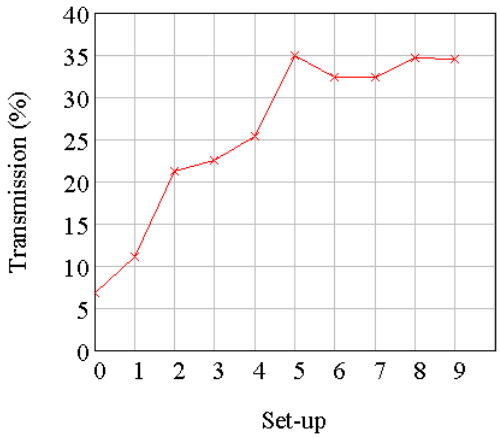

Figure 50: Transmission of various guide set-ups with set-up key again shown in table4.

No:	Set-up	Description
0	IRIS	Parameter set-up for the IRIS instrument
1	OSIRIS	Parameter set-up for the IRIS instrument
2	m2 Curved	dimensionally optimized simple curved guide
3	m3 Curved	dimensionally optimized simple curved guide
4	m2 Elliptic from straight	Full elliptic from the biological shielding
5	m3 Elliptic from straight	Full elliptic from the biological shielding
6	Elliptically tapered m2 curved	Elliptically tapered, dimensionally optimized guide
7	Elliptically tapered m3 curved	Elliptically tapered, dimensionally optimized guide
8	Elliptic vertical (symmetric)	Symmetric full elliptic geometry in the vertical
9	Elliptic vertical (non-symmetric)	Non-symmetric elliptic geometry in the vertical

Table 4: Set-up key

Final conclusions to the investigation indicate that elliptic geometry is the probable choice for guide design with full non-symmetric vertically elliptic and horizontally curved geometry used. However there needs to be further investigation into biological shield modification with the possibility of full elliptic geometry throughout.

Acknowledgments

I acknowledege Dr F. Demmel for support and guidance at the ISIS facility together with advice for the draft project write-up. I would also like to thank Dr S. Ansell for discussion on McStas. I gratefully acknowledge the funding of this project through the ISIS facility enabling my stay at the Rutherford Appleton Laboratory (RAL) for part of my project. I also would like to thank my project supervisor Dr F. Kargl for discussion and advice on the draft write-up and guidance throughout the project.

References

[1] *FIRES (scientific case)*, http://www.isis.rl.ac.uk/molecularSpectroscopy-/fires/FIRES_science.pdf, ISIS Pulsed Neutron and Muon Source, 2008.

[2] Demmel F. and Andersen K.H., *FIRES: a novel neutron backscattering spectrometer*. Meas. Sci. and Tech., 2008. **19**

[3] Willendrup P. et al., *User and Programmers Guide to the Neutron Ray-Tracing Package McStas*, Ris DTU, 2008.

[4] Takahishi N. et al., *A Multiplication of High Energy Resolution*, J-PARC Center, JAEA. 2008.

[5] Takahishi N. et al., *Presentation*, Materials and Life Science Division, J-PARC Center, JAEA. 2008.
http://www.jcns.info/src/ws08/presentations/Bernried_Takahashi.pdf

[6] Laboratory/SNS, O.R.N., *Backscattering Spectrometer (BASIS) at SNS*. http://neutrons.ornl.gov/instrument_systems/beamline_02_basis/index.html.

[7] Telling M., *Monte Carlo simulations of the OSIRIR and IRIS neutron spectrometers using the virtual neutron instrument, VITESS*, Technical Report, RAL-TR-2004-021

[8] Schanzer C. et al., *Advanced geometries for ballistic neutron guides*. Nuc. Inst and Meth. In Phys. Res. SecA, 2004, **529**, 63

[9] Willendrup P. et al., *Component Manual for the Neutron Ray-Tracing Package McStas*, Ris DTU, 2008.

[10] Squires G. L., *Introduction to the Theory of Thermal Neutron Scattering*, Dover Publications Inc., 1997, ISBN 0-486-69447-X.

[11] Klen K., *Simulating Neutron Guides for the European Spallation Source*. Niels Bohr Institute University of Copenhagen. 2008. http://www.fys.ku.dk/∼kaspar/speciale/.

[12] Swissneutronics, http://www.swissneutronics.ch/products-/concept-supermirrors.html.

[13] Well A., Fredrikze H., *On the resolution and intensity of a time-of-flight neutron reflectometer*, Sci. Dir., PhysB, 2005, **357**, 204

[14] *The OSIRIS Primary Spectrometer*, ISIS Molecular Spectroscopy web site, http://www.isis.rl.ac.uk/molecularSpectroscopy/osiris/osiris_primary.htm

[15] Sakai V. et al., *International Conference on Neutron Scattering*, http://www.mrs.org/s_mrs/bin.asp?CID=19203&DID=239718&DOC=FILE.PDF, G4.42 2009.

Appendix A

Items requiring further explanation

IRIS and OSIRIS illustraion

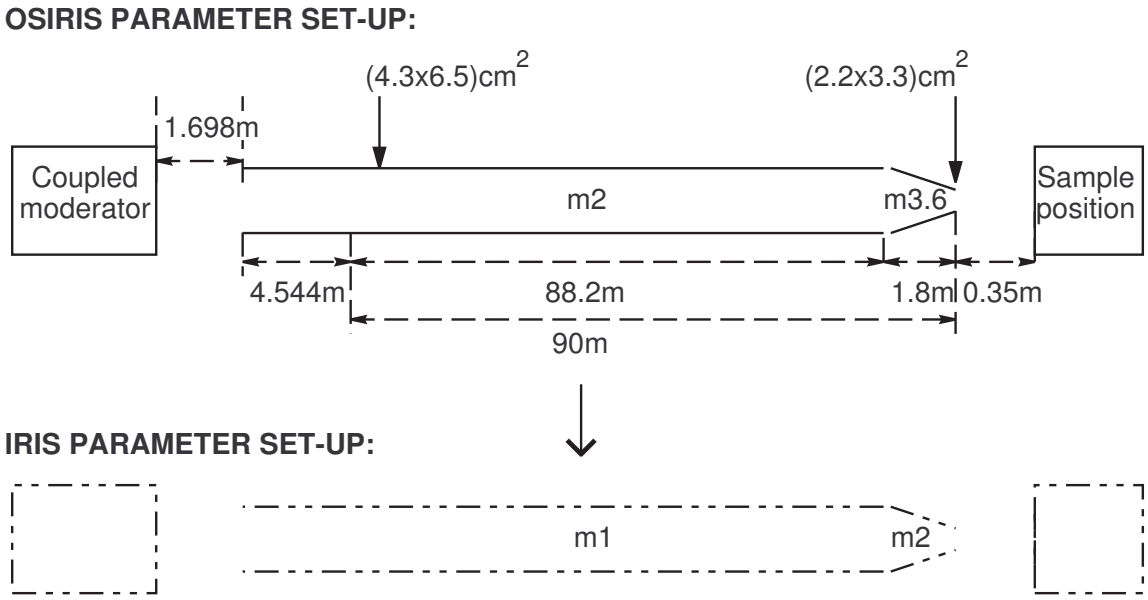

Figure 51: Parameter set-up of both the IRIS and OSIRIS on a 90m long guide for comparison.

Custom elliptically curved guide instrument - Extended

Combining the features of linear tapering, elliptic symmetric or non symmetric and alternate coating distributions is achieved by combining many guide component segments. No such component exists that allows the freedom to create such complex set-ups.

The method to achieve this is by the writing of a FORTRAN program developed as part of this thesis to output an instrument file. Such a program allows the incorporation of user defined features to the guide including curvature, linear tapering and elliptic features in one or both dimensions of the guide.

An elliptic guide in two dimensions is described by different parameters. As such, an elliptic in the horizontal and vertical are independent. An illustration of such a guide is shown in Fig.52.

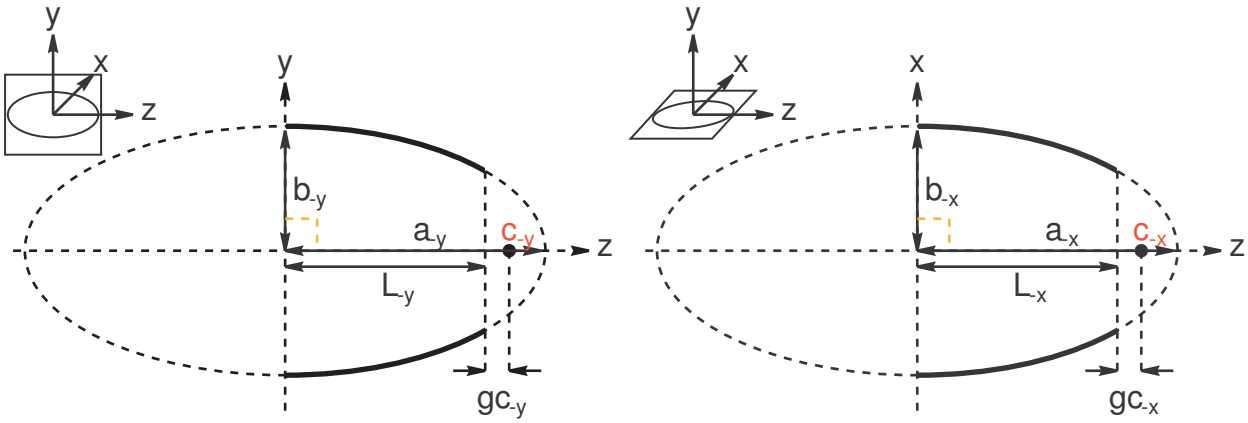

Figure 52: Illustration of a two dimensional elliptic guide along the 'z' axis, where 'c' denotes the foci point, 'gc' the distance from the guide exit to this foci, 'L' the elliptic length, 'b' the minor axis and 'a' the major axis of the ellipse.

The standard expression for an ellipse (lying along the z-axis in the vertical) is defined by Eqn.10;

$$\frac{z^2}{a_y^2} + \frac{y^2}{b_y^2} = 1 \tag{10}$$

Hence;

$$y = \sqrt{b_y^2 \times (1 - \frac{z^2}{a_y^2})}$$

$$\begin{aligned} height(z) &= 2y \\ &= 2\sqrt{b_y^2 \times (1 - \frac{z^2}{a_y^2})} \end{aligned} \tag{11}$$

(See Fig.53) Where;

$$\begin{aligned} c_y &= L_y + gc_y \\ &= \sqrt{a_y^2 - b_y^2} \\ So... \quad a_y &= \sqrt{(L_y + gc_y)^2 + b_y^2} \end{aligned} \tag{12}$$

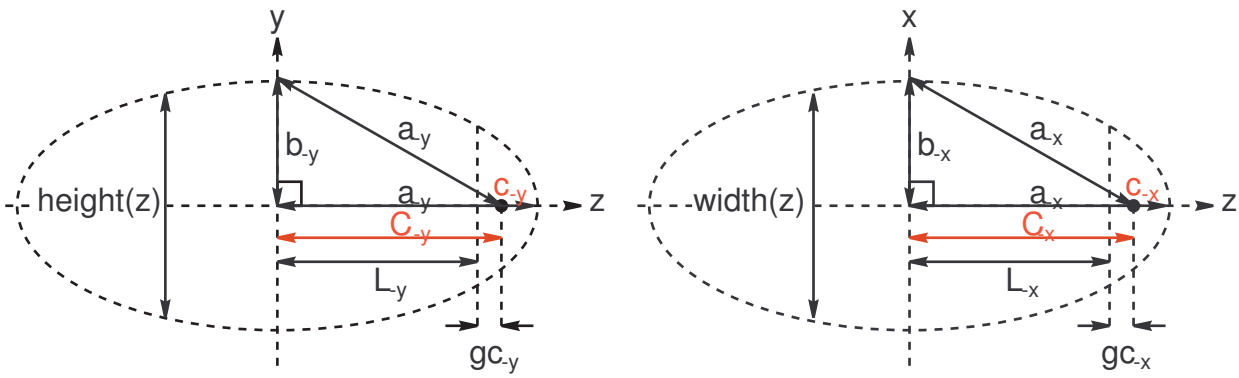

Figure 53:

Similaly for the horizontal ellipse;

$$\begin{aligned} width(z) &= 2x \\ &= 2\sqrt{b_x^2 \times (1 - \frac{z^2}{a_x^2})} \end{aligned} \tag{13}$$

Where;

$$a_x = \sqrt{(L_x + gc_x)^2 + b_x^2} \tag{14}$$

The elliptic guide then is defined by the length 'L', the focal distance 'gc' and finally the minor axis 'b' for both horizontal and vertical dimensions. The elliptic and or curved custom guide is made up from many guide segments and as the eccentricity is so high on such a long guide, segments are larger towards the centre of the guide where the angle is low, but with smaller segments towards the end where the angle gets steeper. As such, an exponential distribution is used to describe the points along the guide as described by Klen K.[11].

The expression used;

$$z = \left[\exp\left(n \frac{\ln(\frac{L_T}{2.0} + 1.0)}{(\frac{N}{2.0})} \right) - 1.0 \right] \tag{15}$$

Where 'N' is the number of segments, 'L_T' the elliptic length and 'n' the segment number (0 to (N/2)-1). This applies to an ellipse starting from its centre point. A looping sequence is used for making a distribution of the above for the rest of the guide

according to the chosen parameters 'N' and 'L_T'. The coating distribution is defined in the same way, and is given by;

$$m = \left[\exp\left(n\frac{\ln(L_T + 1.0)}{(\frac{N}{2.0})}\right) - 1.0\right]\frac{(m2 - m1)}{L_T} + m1 \tag{16}$$

Where 'm2' and 'm1' are the limits of the coating distribution resulting in a exponential distribution between 'm1' and 'm2'. Coating distributions then rounded to the nearest half integers.